Agricultural Water Management 309 (2025) 109356

Contents lists available at ScienceDirect

Agricultural Water Management

journal homepage: www.elsevier.com/locate/agwat

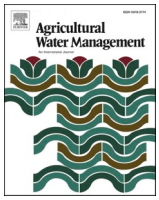

Modeling quinoa growth under saline and water-limiting conditions using SWAP-WOFOST

Diana C. Estrella Delgado [a,*], Tom De Swaef [a], Jan Vanderborght [b,c], Eric Laloy [d], Gerda Cnops [a], Maarten De Boever [a], Abdelaziz Hirich [e], Ayoub El Mouttaqi [e], Sarah Garré [a]

[a] Plant Sciences Unit, Flanders Research Institute for Agriculture, Fisheries and Food (ILVO), Merelbeke-Melle 9090, Belgium
[b] Soil and Water Management Unit, Department of Earth and Environmental Sciences, KU Leuven, Leuven 3001, Belgium
[c] Agrosphere Institute (IBG-3), Forschungszentrum Jülich GmbH, Jülich, Germany
[d] Belgian Nuclear Research Center (SCK CEN), Belgium
[e] African Sustainable Agriculture Research Institute (ASARI), Mohammed VI Polytechnic University (UM6P), Laayoune, Morocco

ARTICLE INFO

Handling Editor: Dr R. Thompson

Keywords:
Abiotic stress
Chenopodium quinoa Willd.
Crop modeling
Parameter estimation
Sensitivity analysis

ABSTRACT

Soil salinization in arid and coastal areas poses a significant threat to crop production, which is further aggravated by climate change and the over-exploitation of aquifers. Cultivation of salt and drought-tolerant crops such as quinoa represents a promising adaptation pathway for agriculture in saline soils. Quinoa (*Chenopodium quinoa Willd.*) is a "salt-loving" plant, known for its tolerance to drought and salinity using complex stress responses. However, available models of quinoa growth are limited, particularly under salinity stress. The objective of this study was to calibrate the crop growth, and salinity and drought stress parameters of the SWAP – WOFOST model and evaluate whether this model can represent quinoa's stress tolerance mechanisms. Field experimental data were used from two quinoa varieties: ICBA-Q5 grown under saline conditions in Laayoune, Morocco, in 2021, and Bastille grown under rainfed, non-saline conditions in Merelbeke, Belgium, from 2018 to 2023. Calibration and parameter uncertainty was performed using the DiffeRential Evolution Adaptive Metropolis (DREAMzs) algorithm on key parameters identified via sensitivity analysis using the Morris method. The resulting crop parameters provide insights into the stress tolerance mechanisms of quinoa, including reduction of transpiration and uptake of solutes. The salinity stress function of SWAP effectively represents these tolerance mechanisms and accurately predicts the impact on yield, under arid conditions. Under Northwestern European climate, the model replicates the impact of drought stress on yield. The calibrated model offers perspectives for evaluating practices to reduce soil salinization in arid conditions and for modeling crop performance under water-limited conditions or future salinization in temperate regions.

1. Introduction

Over 10 % of agricultural land is affected by salinization, particularly in areas already vulnerable such as arid and semi-arid regions (FAO, 2021). In the North Sea coastal regions soil salinization is currently not a major problem for agricultural production. However, these low-lying and fertile coastal regions will be highly vulnerable to seawater inundation from future sea level rise, and from saltwater intrusion caused by groundwater overuse and decreased rainfall (Gould et al., 2021). Tackling these interconnected challenges demands improved irrigation practices, appropriate land management, and the adoption of salt and drought-tolerant crop varieties and/or species adapted to saline environments (FAO, 2021). The cultivation of salt-tolerant crops, called 'saline or biosaline agriculture', is a promising adaptation pathway for agriculture in saline soils, or in situations where irrigation involves brackish or saline water. A comprehensive overview of current research about saline agriculture and numerous case studies illustrating its potential are provided in Negacz et al. (2021).

Drought stress in crops occurs when soil water is insufficient to meet the crop water demand, resulting in suboptimal growth. Salinity stress in

* Corresponding author.
E-mail addresses: diana.estrella@ilvo.vlaanderen.be (D.C. Estrella Delgado), tom.deswaef@ilvo.vlaanderen.be (T. De Swaef), j.vanderborght@fz-juelich.de (J. Vanderborght), eric.laloy@sckcen.be (E. Laloy), gerda.cnops@ilvo.vlaanderen.be (G. Cnops), maarten.deboever@ilvo.vlaanderen.be (M. De Boever), abdelaziz.hirich@um6p.ma (A. Hirich), ayoub.elmouttaqi@um6p.ma (A. El Mouttaqi), sarah.garre@ilvo.vlaanderen.be (S. Garré).

https://doi.org/10.1016/j.agwat.2025.109356
Received 20 August 2024; Received in revised form 24 January 2025; Accepted 1 February 2025
Available online 8 February 2025

crops involves both osmotic and ionic effects (Munns and Tester, 2008). The osmotic effect comes from the salts dissolved in the soil solution around the roots, generating a more negative osmotic potential. Since the root cell membrane acts as a semi-permeable barrier, water movement is controlled by the gradient in osmotic potential between the soil solution and the root cells. A more negative osmotic potential reduces water availability and leads to physiological water stress in plants due to stomatal closure, with a direct effect on the growth of roots and new leaves (Munns and Tester, 2008). In addition, saline-sodic soils often have poor physical and chemical properties, which can further limit water availability (Arora and Dagar, 2019; Bidalia et al., 2019). The ionic effect results from the accumulation of salt ions, namely sodium (Na^+) and chloride (Cl^-), inside the plant, specifically in the leaves, which causes ion toxicity and induces leaf senescence (Munns and Tester, 2008).

Species that are highly susceptible to salinity stress, like most conventional arable crops, are known as glycophytes. Their yields start declining at an electrical conductivity of the saturated soil-paste extract (EC_e) of around 4 dS m^{-1} or even lower (Maas and Hoffman, 1977). However, studies have shown that, even among glycophytes, there are varieties with greater tolerance (Van Straten et al., 2021, 2019), indicating that plants have developed specialized mechanisms to counteract the effects of salinity stress. Halophytes on the other hand are "salt--loving" plants that can tolerate or even thrive in high-salinity environments (Atzori, 2021). They constitute around 2 % of known plant species and are not commonly used for human consumption, except for quinoa (Ruiz et al., 2016).

Quinoa (*Chenopodium quinoa Willd.*) is a pseudo-cereal crop originating from the Andean region of South America, and consumed worldwide thanks to its high nutritional value (De Bock et al., 2022, 2021; Vilcacundo and Hernández-Ledesma, 2017) and adaptability to different climatic conditions. In Northern European countries, such as Denmark, The Netherlands and Germany, new varieties have been developed focusing on high yield, non-bitter seeds, disease resistance, shorter growing period and low photoperiod sensitivity (Jacobsen, 2017; Jaramillo Roman et al., 2021; Präger et al., 2019). In Southern Europe, quinoa varieties have been successfully tested for their adaptability to the Mediterranean climate, resulting in high yield and good quality seeds (Pulvento et al., 2010; Rodríguez Gómez et al., 2021; Yazar et al., 2015). In North Africa, particularly Morocco, several varieties have proven to be well-suited to hot and arid conditions, especially when using irrigation and organic amendments (Bouras et al., 2022; Hirich et al., 2021; Rafik et al., 2021). Quinoa is inherently tolerant to drought and salinity (Ruiz et al., 2016). Quinoa varieties differ in salinity tolerance, but some can tolerate high salinity levels without compromising production or quality (Nanduri et al., 2019; Yazar et al., 2015). Overall, suitable salinity conditions for quinoa are reported between EC = 10 and 20 dS m^{-1} in irrigation water (Hariadi et al., 2011; Lavini et al., 2014; Nanduri et al., 2019).

Quinoa, and other halophytes, have developed complex mechanisms that allow them to tolerate salinity stress. They osmotically adjust to the saline environment and maintain water uptake, by accumulating inorganic ions like Na^+, K^+ and Cl^- in leaf cell vacuoles, and organic compounds (compatible solutes) such as proline and sugars, in the cytosol and organelles, to balance the osmotic pressure in the vacuoles (Adolf et al., 2013; Munns and Tester, 2008; Ruiz et al., 2016). Another mechanism for osmotic adjustment is the reduction of crop transpiration by regulation of the stomatal closure through the production of abscisic acid (ABA) (Adolf et al., 2013) or by decreasing stomatal density (Shabala et al., 2013). Halophytes are also able to maintain an acceptable K^+/Na^+ ratio in the leaves and roots, necessary for optimal cell functioning (Adolf et al., 2013; Munns and Tester, 2008). Other mechanisms involve the activation of enzymatic and non-enzymatic antioxidants, that serve as osmoprotectants (Adolf et al., 2013), the development of external glands called Epidermal Bladder Cells (EBCs) thought to store K^+ and Na^+, water, and organic osmolytes (Koyro and Eisa, 2008; Moog et al., 2022), and the active salt exclusion at the soil-root interface (Kiani-Pouya et al., 2020). The osmotic adjustment and osmoprotection mechanisms in quinoa also contribute to its high drought stress tolerance (Hinojosa et al., 2018). These adaptation mechanisms vary significantly among different crops and varieties, soil and water conditions, and environmental factors (Adolf et al., 2012; Comparini et al., 2024; Jaramillo Roman et al., 2021), and despite extensive research, it still raises numerous questions about the processes involved.

Crop models that include salinity coping mechanisms can improve our understanding of the physiological responses of quinoa to salinity stress in interaction with soil and environmental factors and provide insights into its performance in other regions or future climate. While extensive knowledge exists about salt tolerance mechanisms, the challenge is to effectively represent these mechanisms within crop models. However, the availability of crop models simulating the growth of quinoa (or other halophytes), especially under salinity stress, is limited. Only the SALTMED model has been widely used for simulating the growth of quinoa under saline conditions (Ince Kaya and Yazar, 2016; Peyghan et al., 2020; Pulvento et al., 2013) while AquaCrop and CSM-CROPGRO models have evaluated quinoa only under water-limited conditions (Alvar-Beltrán et al., 2020; Geerts et al., 2009; Präger et al., 2019). AquaCrop does not account for root solute uptake (Raes et al., 2023a), posing a limitation to model halophytes relying on salt inclusion mechanisms for salt tolerance. CSM-CROPGRO does not consider salinity stress and few attempts have been made to adapt the model to saline soils (Webber et al., 2010).

The SWAP-WOFOST model was developed by Wageningen University and Research 50 years ago and contains detailed modules for simulating water and solute transport and different stresses in crops, including drought, oxygen, salinity and frost stress (Heinen et al., 2024). This model is a combination of the soil water transport model SWAP (Kroes et al., 2017) and the crop growth model WOFOST (De Wit et al., 2020). In contrast to AquaCrop, SWAP simulates salt uptake, making it suitable for modeling the evolution of soil salinity in fields where halophytes are grown. Salt uptake is a function of the root water uptake, the concentration of salts in the pore water, and a factor that represents either salt exclusion or active salt uptake. SWAP-WOFOST uses the simple salinity stress function proposed by Maas and Hoffman (1977), which reduces crop transpiration with increasing soil salinity concentration in the root zone. This salinity stress function depends solely on the soil salinity concentration and not on the plant internal salt content; therefore, stress due to toxicity effects are not directly accounted for. Despite its limitations, this linear function has been extensively used and continues to be employed in several models thanks to its simplicity. In the last decades, more detailed functions and approaches have been proposed as alternatives, such as the S-shaped function of Van Genuchten and Hoffman (1984), the nonlinear equation of Misle and Kahlaoui (2015) that describes osmotic and ionic effects, or the inclusion of osmotic stress in the calculation of root water uptake (Dalton et al., 1975; De Jong van Lier et al., 2009).

A first objective of this study is to explore the potential of a combination of a salt uptake function with the Maas and Hoffman (1977) function to capture the salinity stress in quinoa. Therefore, we calibrated crop, salt uptake, and salinity and drought stress parameters of the SWAP - WOFOST model using field experimental data from the arid region of Laayoune (Morocco) under irrigation with different salinity levels. A second objective is to derive crop and drought stress parameters for a different quinoa variety in Merelbeke (Belgium), under rainfed and non-saline conditions. By doing so, we aim to facilitate research in current or future saline soils, and support simulation of drought stress in quinoa.

2. Materials and methods

2.1. Field experiments

2.1.1. Quinoa in Laayoune (Morocco) under saline conditions

Quinoa (*Chenopodium quinoa Willd.)*, variety ICBA-Q5, was cultivated in the experimental farm of the National Institute of Agricultural Research in Foum El Oued area, Laayoune, in the south of Morocco (lat = 27.186°, lon = −13.341°), from 13 April 2021 to 29 July 2021. ICBA-Q5 was bred by the International Center of Biosaline Agriculture (ICBA) in the UAE. Laayoune has a dry and hot climate, highly influenced by the ocean. During the experiment, the minimum average temperature was 18 °C and maximum average temperature was 25 °C, and the total precipitation was only 7 mm. Because precipitation is low and the coastal aquifers are saline, agriculture relies on irrigation with saline water. The soil was irrigated using drip irrigation, with a flow rate of 2 L h^{-1} (~8 mm), twice a week. Between sowing and crop emergence, irrigation water had a salinity level of 4 dS m^{-1}. After crop emergence (two weeks after sowing), three irrigation treatments with different salinity levels: EC_{water}= 4 dS m^{-1}, 12 dS m^{-1} and 20 dS m^{-1}, were adopted. The total irrigation amount applied during the growing season, for each of the three treatments, was 240 mm. The soil is a sandy loam with high salinity and low organic carbon (Table 1). We used a factor of 1.72 to estimate organic matter from organic carbon, as required by SWAP.

Available data for model calibration consisted of dry biomass and yield, soil water content (θ) at 10 cm depth and soil electrical conductivity of the saturated soil-paste extract (EC_e) at 10 cm depth, for 2021. Soil water content (θ) and bulk soil EC were measured using Decagon TEROS 10 and 12, from 25 May 2021 onwards. The bulk soil EC was further processed and provided as EC_e (Meter, 2018). In turn, we converted EC_e to soil salinity concentration (c), as required for the model input, using a conversion factor that depends on the magnitude of EC (see supplementary materials). This allows to partially account for the non-linear relationship between EC and soil salinity concentration, especially at high salinity levels.

The experiment was originally designed to test the effect of nine different organic amendments on tolerance to salinity stress. For the modeling tasks, we simplified the dataset to focus solely on the irrigation water salinity, taking each time the average yield and biomass of all amendments. This decision was made due to significant variations among amendments and the lack of a nutrient simulation module in SWAP. Soil water content and electrical conductivity EC_e were only available for the sheep manure amendment for the three salinity levels. Further details about the experiment are available in El Mouttaqi et al. (2023).

2.1.2. Quinoa in Merelbeke (Belgium) in rainfed and non saline conditions

Quinoa field experiments were conducted at the Flanders Research Institute for Agriculture, Fisheries and Food (ILVO) in Merelbeke, Belgium (lat = 50.983°, lon = 3.769°), from 2018 to 2023 (De Bock et al., 2022, 2021; ILVO, 2023). The climate in the experimental site is characterized by mild temperatures and moderate to high precipitation, typical of the North-West European climate. Between the growing seasons of 2018 and 2023, the average maximum temperature was 22 °C and the average minimum temperature was 11 °C, and precipitation varied from 163 mm in 2022–327 mm in 2023. The field experiments comprised several nitrogen (N) fertilization treatments and varieties, grown without irrigation and under non-saline conditions.

For calibration, we selected only the variety Bastille under 100–130 kg N ha^{-1} fertilisation treatment (optimal nutrient supply). Bastille is an early variety bred by Radicle Crops, which has consistent yields and good disease resistance under Flemish conditions. Bastille seeds were provided by Radicle Crops through a Material Transfer Agreement (MTA). We used dry yield measurements collected from four replicate plots across the growing seasons of 2018, 2019, 2022 and 2023. The length of the growing season was on average 136 days, with plants reaching an average maximum height of 100 cm. In addition, soil water content (0–30 cm, 30–60 cm, 60–90 cm depth) and Leaf Area Index (LAI) were available for 2023, for each replicate plot. Gravimetric water content was measured manually every two weeks by soil sampling and weighing before and after oven-drying (105 °C for 24 h), and then converted to volumetric water content using the measured bulk density. LAI was measured every week using the SunScan Canopy Analysis System type SS1.

Soil texture is mostly sandy loam with low organic carbon (Table 2). The groundwater level in the experimental field, measured at the start of the growing season in 2023, was on average 1.95 m deep in the whole field. This value was assumed the same for all the years in the calibration process.

2.2. SWAP - WOFOST model

SWAP (Soil, Water, Atmosphere and Plant) is a 1-D field scale model simulating the transport of water, solutes and heat in the unsaturated and saturated zone, in interaction with crop development (Kroes et al., 2017). The dynamic crop growth module WOFOST (World Food Studies) is integrated in SWAP to describe the phenological development, growth and yield production of major arable crops (De Wit et al., 2020).

2.2.1. Soil water and solute transport

SWAP computes the transport of water, solutes and heat in the unsaturated and saturated zone using the Richards equation (Eq. (1)), including root water extraction to simulate the movement of soil moisture in variably saturated soils.

$$\frac{\partial \theta}{\partial t} = \frac{\partial}{\partial z}\left[K(h)\left(\frac{\partial h}{\partial z} + 1\right)\right] - S_a(h) \quad (1)$$

Where θ is the volumetric water content ($cm^3\ cm^{-3}$), t is time (d), $K(h)$ is the hydraulic conductivity (cm d^{-1}) as function of the soil water

Table 1
Soil texture, organic carbon and electrical conductivity of the sandy loam soil in the experimental field in Laayoune.

z[a] cm	BD[b] mg cm^{-3}	Clay[c]%	Silt[d]%	Sand[e]%	OC[f]%	EC_e[g] dS m^{-1}
300	1600	18.6	19.6	61.8	0.273	9.55

[a] Soil layer depth.
[b] Bulk density.
[c] Percentage of clay (<0.002 mm).
[d] Percentage of silt (0.002 – 0.05 mm).
[e] Percentage of sand (0.05 – 2 mm).
[f] Organic carbon.
[g] Soil electrical conductivity of the saturated soil-paste extract.

Table 2
Soil texture and organic carbon for the sandy loam soil in the experimental field in Merelbeke.

z[a] cm	BD[b] mg cm^{-3}	Clay[c]%	Silt[d]%	Sand[e]%	OC[f]%
35	1469	6.8	36.6	56.6	0.78
60	1644	8.2	51.9	39.9	0.49
300	1668	8.2	51.9	39.9	0.49

[a] Soil layer depth.
[b] Bulk density.
[c] Percentage of clay (<0.002 mm).
[d] Percentage of silt (0.002 – 0.05 mm).
[e] Percentage of sand (0.05 – 2 mm).
[f] Organic carbon.

pressure head, h (cm), z is the soil depth (cm) taken positive upward, and S_a is the actual root water uptake ($cm^3\ cm^{-3}\ d^{-1}$). This equation is solved numerically in SWAP by discretizing the soil in compartments and by using the Mualem-Van Genuchten functions (Mualem, 1976; Van Genuchten, 1980) that relate h, θ and K. The top boundary conditions of the system are characterized by the vegetation coverage and the atmospheric conditions. The bottom boundary condition describes the interactions between the soil profile, at the bottom boundary of the modelled soil column, and the underlying groundwater or deeper soil layers (Kroes et al., 2017). We selected "*Free drainage of soil profile*" as the bottom boundary condition for Laayoune due to the deep groundwater (~25 m), and "*Prescribed soil water pressure head of bottom compartment*", as condition for Merelbeke. The pressure head of the bottom compartment is the height of the groundwater level relative to the depth of the bottom soil compartment.

The soil hydraulic parameters for Laayoune and Merelbeke, shown in Table 3, were derived from existing databases and literature, and adjusted if necessary to ensure satisfactory agreement between simulated and observed soil water content.

SWAP simulates the transport of a single species or solute to approximate the dynamics of all species in the soil solution. We assumed that all species that are represented by this single solute have the same contribution to the electrical conductivity (EC) or osmotic potential. Even though individual cations adsorb to negatively charged soil particles (such us clay plates), adsorption of one ion corresponds with a desorption of another, so the total equivalent concentration is not influenced by sorption and desorption. Therefore, EC or osmotic potential does not depend on the composition of the solution but only on its total equivalent concentration. We parameterized the model so that this single solute behaves as a conservative solute. This means that it does not undergo chemical reactions, adsorption, dissolution or precipitation. Therefore, we used a simplified solute transport equation (Eq. (2)) that considers only convection, dispersion and root solute uptake. The convective flux represents the solutes carried along with the moving water, while the dispersion flux accounts for the dispersion caused by velocity variations in the soil porous medium (Kroes et al., 2017). The solute concentration in the root zone is determined using the principle of mass conservation.

$$\frac{\partial(\theta c)}{\partial t} = -\frac{\partial(qc)}{\partial z} + \frac{\partial\left[\theta(D_{dis})\frac{\partial c}{\partial z}\right]}{\partial z} - K_r S_a c \tag{2}$$

Where, θ is the volumetric water content ($cm^3\ cm^{-3}$), c is the salinity concentration in the soil solution ($mg\ cm^{-3}$), t is time (d), q is the Darcy flux ($cm\ d^{-1}$), z is the soil depth (cm) taken positive upward, $D_{dis} = L_{dis}\left|\frac{q}{\theta}\right|$ is the dispersion coefficient ($cm^2\ d^{-1}$), L_{dis} is the dispersion length (cm) set to 5 cm (default), K_r (or TSCF in the model files) is the root uptake preference factor (-), and S_a is the actual root water uptake ($cm^3\ cm^{-3}\ d^{-1}$).

The term $K_r S_a c$ reflects the rate at which the solutes are taken up by the roots. The factor, K_r (TSCF), represents the preference of the plant for taking up solute ions relative to the amount of water extracted from the soil. A value equal to zero means that there is a complete salt exclusion, while a value equal to 1 indicates that solutes are taken up proportional to their concentration in the water. A value larger than 1 means that more salts are extracted by the roots than what flows in with the water. This factor was included in the calibration process.

2.2.2. Transpiration reduction due to drought and/or salinity stress

Potential transpiration (T_{pot}) and potential soil evaporation (E_{pot}) are calculated based on direct application of Penman-Monteith equation (equations 3.17 and 3.16 of the SWAP manual) (Kroes et al., 2017).

The potential soil evaporation (E_{pot}) depends on the soil resistance of a wet soil (RSOIL), which was calibrated. When the topsoil is wet, water evaporates freely and actual soil evaporation (E_{act}) equals E_{pot}. As the topsoil dries and its hydraulic conductivity decreases, E_{act} becomes limited by the maximum soil evaporation rate ($E_{\max}$), which is determined by the hydraulic properties of the topsoil layer. In addition, an empirical reduction function can be used to account for variations in topsoil hydraulic properties. We used the empirical function of Boesten and Stroosnijder (1986) (with empirical coefficient β_2 or COFRED = 0.54 $cm^{1/2}$, default). The actual evaporation (E_{act}) is then calculated as the minimum between E_{pot}, $E_{\max}$ and this empirical value.

The potential transpiration (T_{pot}) represents the maximum transpiration rate based on atmospheric conditions and plant characteristics, under optimal soil water, nutrient and temperature conditions (Kroes et al., 2017). The potential transpiration depends on the minimum canopy or stomatal resistance ($r_{s,\ \min}$ or RSC), which was calibrated. T_{pot} is distributed over the rooting depth, based on the root length density at the specific depth (z), which gives the potential root water uptake (S_{pot}). The actual root water uptake (S_{act}) is then calculated from S_{pot}, and reduced by stress factors (Eq. (3)). The actual root water uptake integrated over the rooting depth is equal to actual transpiration (T_{act}). The factors α_{rw}, α_{rd}, α_{rs} and α_{rf} correspond to oxygen, drought, salinity and frost stress, respectively. In this study, only drought and salinity stress were considered.

$$S_{act}(z) = \alpha_{rw}\ \ \alpha_{rd}\ \ \alpha_{rs}\ \ \alpha_{rf}\ \ S_{pot}(z) \tag{3}$$

Drought stress results from insufficient water in the root zone to meet the crop water demand, leading to reduced root water uptake. The drought stress factor, α_{rd}, is calculated by the function of Feddes et al. (1978) (Eq. (4)). Above h_3, root water uptake is optimal, and no drought stress occurs. Below h_3, the root water uptake linearly decreases until zero at h_4 (wilting point). The term h_3 is split into two thresholds based on the atmospheric demand, h_{3l}andh_{3h}, since water stress will start earlier at higher transpiration demand. The parameters h_{3l} and h_{3h} (HLIM3L and HLIM3H respectively), were included in the calibration process. The parameter h_4 (HLIM4) was assumed equal to −10000 cm (default).

Table 3
Soil hydraulic parameters for the sandy loam soils in the experimental fields of Laayoune and Merelbeke.

Location	z[a] cm	θ_r[b] $cm^3\ cm^{-3}$	θ_s[c] $cm^3\ cm^{-3}$	α[d] cm^{-1}	n[d] -	K_{sat}[f] $cm\ d^{-1}$	$L_{exp}(\lambda)$[d] -	h_e[e] cm
Laayoune	300	0.01	0.395	0.0068	1.245	43.7	−2.489	0
Merelbeke	35	0.01	0.42	0.0163	1.559	54.8	0.177	0
Merelbeke	60	0.01	0.39	0.0163	1.559	8.64	−0.904	0
Merelbeke	300	0.01	0.40	0.0248	1.321	8.64	−0.904	0

[a] Soil layer depth.
[b] Residual water content.
[c] Saturated water content.
[d] Empirical shape parameters.
[e] Saturated hydraulic conductivity.
[f] Minimum capillary height for modification near saturation.

$$\alpha_{rd} = \begin{cases} 1 & h \geq h_3 \\ \dfrac{h - h_4}{h_3 - h_4} & h_4 < h < h_3 \\ 0 & h \leq h_4 \end{cases} \quad (4)$$

Salinity stress results from an excess of dissolved solutes in the soil solution around the roots (more negative osmotic potential), leading to reduced water uptake and hence crop transpiration. SWAP calculates the salinity stress factor, α_{rs}, using the function of Maas and Hoffman (1977) (Eq. (5)), which is widely used due to its requirement of only two parameters, $S_{\max}$ and S_{slope}. It assumes that above a certain salinity threshold ($S_{\max}$), the transpiration is linearly reduced with increase of soil salinity concentration, with a rate S_{slope}. As long as the salinity concentration in the soil solution does not excess $S_{\max}$, α_{rs} is equal to 1 and the root water uptake is not affected by salinity stress. When the salinity concentration is higher, α_{rs} will be lower than 1, following the linear reduction function. The parameters $S_{\max}$ and S_{slope}, referred as SALTMAX and SALTSLOPE in the model files, were included in the calibration process, for the Moroccan site only.

The salinity stress function focuses solely on how salts directly affect transpiration and crop growth through osmotic effects. However, toxic effects might be implicitly included in the SALTMAX and SALTSLOPE parameters (Werkgroep Waterwijzer Landbouw, 2018).

$$\alpha_{rs} = \begin{cases} 1 & c \leq S_{\max} \\ 1 - S_{slope}(c - S_{\max}) & c > S_{\max} \end{cases} \quad (5)$$

The root system and soil properties determine the available water and nutrients for plant growth. In SWAP, the development of the rooting depth over time, assuming no soil restrictions, can be described by the initial rooting depth (RDI), the maximum rooting depth (RDC), and the maximum daily increase (RRI). The actual rooting depth over time is also function of the relative increase in dry matter. The relative root density distribution is constant and follows a linear relationship that is maximal near the soil surface and decreases to zero at the actual rooting depth. Drought or salinity stress does not affect the distribution of roots in the root zone, but do influence crop growth and rooting depth. In reality, suboptimal soil conditions will impact both root density distribution and water uptake patterns. Root growth may be restricted or absent in very dry or saline soil layers, or water uptake may increase in sparsely rooted but optimal soil layers to compensate for reduced uptake in densely rooted but suboptimal soil layers (Jarvis, 2011). To reflect this dynamic root water uptake, SWAP allows the application of a compensation factor, ALPHACRIT, in the transpiration reduction (Jarvis, 2011, 1989). This factor is a critical threshold in the range 0–1, with 1 meaning that stress occurs as soon as the conditions somewhere in the root zone are not optimal (no compensation), leading to an immediate reduction in crop transpiration. Values below 1 indicate that transpiration continues at the potential rate, even in the presence of stress, until this critical threshold is reached (T_{act}/T_{pot} < ALPHACRIT) and transpiration starts to reduce. This compensation factor increases transpiration by a factor 1/ALPHACRIT compared to no compensation (Heinen et al., 2024; Jarvis, 2011). We used the default value of ALPHACRIT = 0.7, for both drought and salinity stress, as proposed in the crop files available in the SWAP documentation.

2.2.3. Crop growth

The dynamic crop growth WOFOST implemented in SWAP, describes the phenological development, growth, and yield formation of major arable crops. It calculates how much light and CO_2 is intercepted and potentially converted by photosynthesis into carbohydrates, which are the building blocks for biomass production. This potential photosynthesis is reduced by different stress reduction factors (drought and salinity stress, with compensation, in this case) to obtain the actual photosynthesis. The energy captured during photosynthesis is used for maintenance respiration and conversion into dry matter. During this conversion, some energy is lost as growth respiration. The dry matter produced is distributed over the different parts of the crop: roots, stems, leaves and storage organs, based on partitioning coefficients and the development stage of the crop (DVS). The dry matter allocated to leaves subsequently influences how much light can be intercepted. Due to all these complex interactions, feedback mechanisms and crop physiological responses, there is not a linear relationship between transpiration reduction and yield reduction. DVS depends on the temperature sum, while other processes like the distribution of assimilates or crop senescence are controlled by DVS. DVS varies from 0 to 2, with DVS = 0 at emergence, DVS = 1 at flowering and DVS = 2 at maturity (De Wit et al., 2020).

2.3. Model calibration approach

Our model calibration approach for obtaining the new quinoa crop parameters involved the following steps:

1. Defining a "plausible" range of parameter values for quinoa using the available data and literature.
2. Running a sensitivity analysis with the plausible parameter ranges as a basis, to identify the most important ones affecting the output of interest.
3. Calibrating the key parameters, using the DREAMzs algorithm with experimental data from the field.
4. Assessing calibration performance via statistical indices, and model parameter uncertainty.

2.3.1. Defining "plausible" parameter range

De Wit and Boogaard (2021) and De Wit and Wolf (2010) provide clear guidelines for the calibration procedure of WOFOST parameters, which parameters are commonly the most sensitive ones, and their range of variation. This range of variation was used as the plausible parameter range for sensitivity analysis and calibration (Table A.1 in appendix). For parameters not included in De Wit and Boogaard (2021), we used the range of variation provided inside available crop and swap files, with adjustments made where possible based on observed data.

2.3.2. Morris method for sensitivity analysis to identify target parameters

Sensitivity analysis is a method to identify which of the numerous parameters in a model exhibit the most substantial influence on the model's output of interest. Contrary to calibration, this analysis is independent of available observations. We used the Global Sensitivity Analysis method developed by Morris (1991) and enhanced by Ruano et al. (2012), available in the SALib python package (Herman and Usher, 2017; Iwanaga et al., 2022; SALib, 2024), to assess the significance of various crop parameters in the yield, biomass, transpiration and root solute uptake.

The Morris method uses a set of trajectories to randomly sample the parameter space, which is scaled to the interval [0,1]. Each parameter ($x_1,\ldots,x_n$) can only take values at p evenly spaced intervals or grid levels $[0,\ 1/(p-1),\ 2/(p-1),\ \ldots,\ 1]$, which allows efficient exploration of the parameter space with few samples. Each trajectory involves perturbing one parameter at a time ($k = 1, 2, \ldots, n$), by a fixed step size, $\Delta = \frac{p}{2(p-1)}$, while keeping the others fixed, until all the n parameters have been changed. For each parameter, Morris calculates the elementary effects (EE_k), which represents the change in the model output ($f(\boldsymbol{x})$) due to small perturbations in that parameter (x_k) (Eq. (6)). The parameter samples are scaled back to their original values based on their respective parameter range before being evaluated in the model.

$$EE_k = \frac{f(x_1,\ldots,x_k+\Delta,\ldots,x_n) - f(x_1,\ldots,x_k,\ldots,x_n)}{\Delta} \quad (6)$$

The Morris method computes two sensitivity indices:

- **Mean of the absolute elementary effects for each parameter (μ^*)**: represents the average sensitivity of the parameter.
- **Standard deviation of the absolute elementary effects for each parameter (σ)**: represents non-linear effects and interactions with other parameters.

Parameters with larger μ^* are deemed more sensitive as they contribute more to changes in the model output. Parameters with greater σ are considered to either exhibit non-linear behaviour (changes in the parameter do not produce a proportional change in the model output) or have interactions with other parameters.

We selected 100 trajectories and 8 grid levels (p) for parameter sampling based on earlier experience (Coudron et al., 2021), and a total of 30 crop parameters (Table A.1 in Appendix) following the WOFOST guidelines (De Wit and Boogaard, 2021). To make the elementary effects comparable between model outputs, we scaled them by the ratio of the standard deviation of the parameter to the standard deviation of the model output, according to Sin and Gernaey (2009), and available in the SALib package.

2.3.3. DREAMzs (differential evolution adaptive metropolis) for parameter estimation

DREAM is a sampling algorithm used in Bayesian statistical inference that derives the posterior parameter distribution given the observed data and available prior information. The core of Bayesian inference is that the posterior parameter distribution can be approximated from the prior parameter distribution and the likelihood function (Eq. (7)). Therefore, the posterior distribution combines previous knowledge of the parameters of interest and the observations (Vrugt, 2016).

$$p(x|Y) \propto p(x)p(Y|x) \tag{7}$$

$p(x|Y)$ represents the posterior probability of the parameters x conditioned to the observations Y, $p(x)$ is the prior probability of those parameters, and $p(Y|x)$ is the likelihood, that is, the probability of Y being generated from the parameters x.

The prior distribution contains all the knowledge about the parameters. Prior distributions can be assumed uniform (equal probability for all parameter values), normal with or without correlation, among others (Vrugt, 2016). The likelihood function commonly assumes that the error residuals (the difference between observed and simulated values) are non-correlated or random, and normally distributed, and can be used for either homoscedastic or heteroscedastic measurement errors (Vrugt, 2016). The terms "homoscedastic" and "heteroscedastic" refer to constant or variable errors, respectively, in the observed variable.

The posterior distribution is sometimes complex, high-dimensional and with several local optima, and consequently, cannot be estimated analytically. Markov Chain Monte Carlo (MCMC) simulation methods are frequently used for sampling the posterior distribution. The DREAMzs algorithm (Laloy and Vrugt, 2012; ter Braak and Vrugt, 2008; Vrugt et al., 2009) is an improved MCMC approach, which runs multiple chains or trajectories simultaneously to explore the parameter space until convergence to a steady distribution has been achieved. Monitoring this convergence is done simultaneously for all the parameters with the multivariate $\widehat{R}$-statistic of Gelman and Rubin (1992). The convergence is declared when this statistic is smaller than 1.2. Together with the $\widehat{R}$-statistic, the rate of acceptance (AR) of the proposals is also monitored. Values ranging between 15 % and 40 % indicate a satisfactory performance of the algorithm.

The output of DREAMzs is the posterior parameter distribution, which under certain conditions consists of a representative set of all plausible parameter values given the observations and available prior information. The parameter set with maximum a posteriori (MAP) probability is the derived most probable parameter given the observations and prior information. The parameter set with maximum likelihood (ML) is the parameter set that leads to the best fit to the observed data, among the collected posterior samples. This approach allows to assess the uncertainty of the estimated parameters so that the uncertainty of model predictions due to the parameter uncertainty can be evaluated. This is a crucial advantage when availability of experimental data is scarce.

For the calibration, we assumed a 'normal' prior distribution for all calibrated parameters, restricted to the parameter space (Table A.1 in Appendix). The mean of this distribution was the best parameter value derived from available data, literature, and initial fine-tuning of the model, prior to the actual Bayesian inversion. The standard deviation was assumed 30 % of the mean. The error in the observations, used in the likelihood function, was assumed constant for every observation variable as follows: 0.05 $cm^3\ cm^{-3}$ for soil water content, 5 mg cm^{-3} for soil salinity concentration, 0.5 $cm^2\ cm^{-2}$ for LAI, 250 kg ha^{-1} for yield and 500 kg ha^{-1} for biomass.

2.3.4. Additional considerations for model calibration

Ideally, model calibration should first be done under non-stressed conditions, comprising parameters related to the length of the phenology stages, light interception and potential biomass production, and assimilate distribution between crop organs. Once these parameters for potential production are defined, the remaining parameters related to the stress functions can be calibrated. However, the available data consisted only of observations under stressed conditions (salinity and drought stress). Therefore, the calibration was done in one single step, involving both potential production and stress-limited production parameters.

In WOFOST, there are scalar and tabular parameters. Scalar parameters are just one value, while tabular parameters vary with development stage (DVS). The calibration of tabular parameters such as partitioning coefficients, can be done through logistic functions (see supplementary materials). The specific leaf area (SLA) and maximum CO_2 assimilation rate (AMAX) also vary with DVS, but we opted for a simpler calibration approach to avoid too many parameters. We assumed that their values remained constant until DVS = 1 (start of flowering), followed by a linear decline until reaching 0 at DVS = 2 (maturity). These values were found via calibration.

2.3.5. Statistical indices for assessing model performance

We used three statistical indicators to evaluate quantitatively the model simulations, the root mean square error (RMSE, Eq. (8)), the normalized root mean square error (NRMSE) calculated by dividing RMSE by the mean of the observations, and the coefficient of determination (R^2, Eq. (9)). Each one of these indicators considers different kinds of model uncertainties. The RMSE statistic measures the average deviation of the simulations ($\hat{y}$) from the observations (y), expressing the model deviation (bias) and the variance of the random errors. It ranges between 0 and infinite, with 0 meaning a perfect fit. The metric NRMSE is dimensionless and varies from 0 to 1, allowing comparisons between observational variables. The coefficient of determination R^2 measures how good the variance of the observed values is explained or predicted by the model. It is dimensionless and normally ranges from 0 to 1, with 1 meaning a perfect fit. Negative values are also possible, which indicates that the model is a worse predictor than the mean of the observations. These metrics have the limitation that are overly sensitive to high values or outliers and do not differentiate between over- and underestimation (Raes et al., 2023b). Therefore, they constitute a complement to the graphical comparison between modeled and observed values.

$$RMSE = \sqrt{\frac{1}{n}\sum_{i=1}^{n}(y_i - \hat{y}_i)^2} \tag{8}$$

$$R^2 = 1 - \frac{\sum_{i=1}^{n}(y_i - \hat{y}_i)^2}{\sum_{i=1}^{n}(y_i - \bar{y})^2} \tag{9}$$

Where, $\bar{y}$ is the mean of the observations and n the number of obser-

vations.

3. Results

3.1. Sensitivity analysis

Fig. 1 shows the ranked average sensitivity (μ^*) of the parameters, for yield and solute uptake under low (EC = 4 dS m^{-1}) and high salinity (EC = 20 dS m^{-1}) in Laayoune, while Fig. 2 illustrates the ranked average sensitivity for yield and transpiration, in Merelbeke. The results showing also the non-linear effects and interactions between parameters (σ), for all the output variables, are given in supplementary materials. The larger the μ^* value for a certain parameter, the more sensitive is the model output to changes in that parameter. Fig. 1 shows that SALTSLOPE, SLA, SALTMAX, AMAX, TSUMEA and FRTBa are the most sensitive parameters in most situations. This sensitivity slightly changes depending on the model output (e.g. yield, solute uptake) and conditions (e.g. salinity levels). For example, under high salinity, SALTSLOPE and TSUMEMEOPT becomes notably more sensitive. Similarly, parameters TSCF and RSC have a greater influence on the root solute uptake than on the other model outputs. In Merelbeke (Fig. 2), similar to Laayoune, parameters TSUMEA, AMAX, SLA, RSC and FRTBa are the most sensitive for all output variables analysed, over the years 2018, 2019, 2022 and 2023. In addition, FOTBm is highly influential for yield, while SPAN is a sensitive parameter for transpiration. In general, parameters with a higher μ^* also show larger non-linear effects on the model output and interactions with other parameters (Fig. S.1 and Fig. S.2 in supplementary materials). The parameters HLIM3L, HLIM3H, Q10, RMO, RRI, RDI, FRTBb, FOTBb and FLTBb, are the least sensitive for all the model outputs and conditions analysed.

3.2. Parameter estimation

Based on the sensitivity analysis and data availability, 17 parameters were calibrated using DREAMzs for the Moroccan case (Fig. 1), and 13

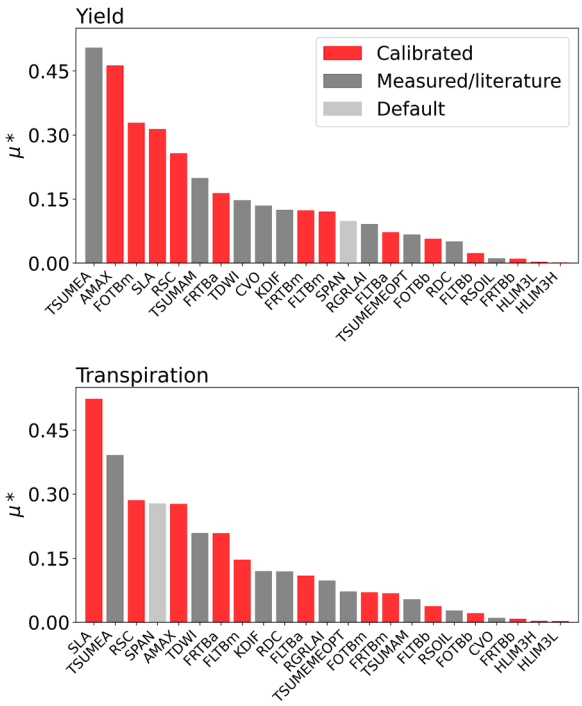

Fig. 2. Ranked average sensitivity (μ*) given by the Morris method, on yield and transpiration, for the Belgian case, averaged over the years 2018, 2019, 2022 and 2023. Parameters selected for calibration are depicted in red, those estimated from observations or literature available for quinoa are shown in dark grey, and parameters obtained from default WOFOST potato file, are displayed in light grey. Some non-sensitive parameters have been omitted to improve visualization. For a description of all the parameters, refer to Table A.1 and Table A.2 in appendix.

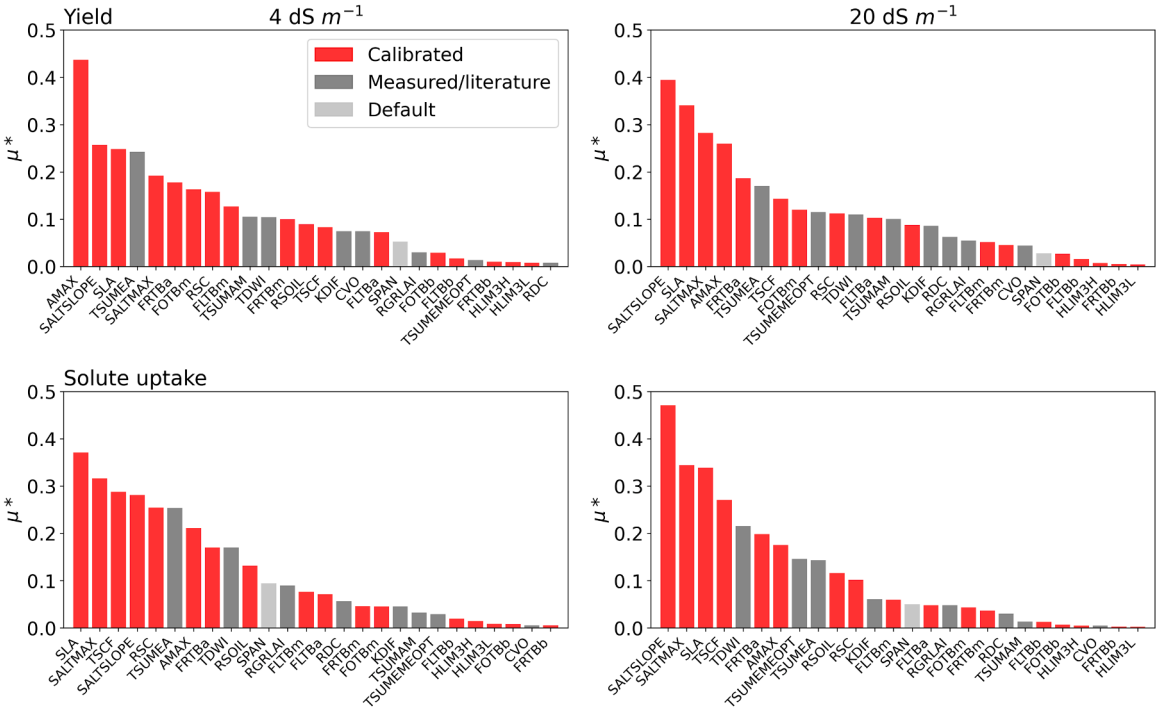

Fig. 1. Ranked average sensitivity (μ*) by the Morris method, on yield and solute uptake, for the Moroccan case, under low (4 dS m^{-1}) and high salinity (20 dS m^{-1}) in irrigation water. Parameters selected for calibration are depicted in red, those estimated from observations or literature available for quinoa are shown in dark grey, and parameters obtained from the default WOFOST potato file, are displayed in light grey. Some non-sensitive parameters have been omitted to improve visualization. For a description of all the parameters, refer to Table A.1 and Table A.2 in appendix.

parameters for the Belgium case (Fig. 2), which does not include salinity stress. Some of these parameters, such as drought stress parameters (HLIM3L, HLIM3H) and partitioning coefficients were included in the calibration despite most of them having low influence, due to the lack of available information in the literature for quinoa. Other parameters including the sum of the temperature (TSUMEMOPT, TSUMEA, TSUMAM), initial crop weight (TDWI), maximum rooting depth (RDC), relative increase of LAI (RGRLAI), extinction coefficient (KDIF) and conversion efficiency (CVO) were derived from the available measurements or literature. For the remaining crop parameters, values were adopted from the default WOFOST potato file. The parameters drawn from the default WOFOST potato file are mostly general parameters that are very similar or even the same between different crops (e.g. potato, winter wheat, maize, barley and sugar beet). Table A.2 in the appendix contains the calibrated parameters for ICBA-Q5 and Bastille, as well as other crop parameters estimated from literature or available data.

There are crucial differences between these two varieties, regarding phenological development, transpiration and yield production. The main differences rely on the temperature requirement for reaching emergence (TSUMEMEOPT) and flowering (TSUMEA), the minimum stomatal resistance (RSC), the maximum CO_2 assimilation rate (AMAX), the allocation of dry matter to the different plant organs (FRTB, FLTB, FOTB) and drought stress parameters (HLIM3H, HLIM3L). Compared to Bastille, the variety ICBA-Q5 has a higher TSUM requirement, especially for reaching flowering, exhibits a greater stomatal resistance and a lower CO_2 assimilation rate. Additionally, it allocates less dry matter to roots and more to above-ground biomass, particularly to leaves, and it also demonstrates slightly higher drought tolerance (Fig. 3).

The salinity stress parameters, calibrated only for the ICBA-Q5 variety under the agro-climatic conditions of Laayoune, indicate that SALTMAX is 5.1 mg cm^{-3} and SALTSLOPE is 0.0103 cm^{-3} mg. Using the conversion procedure detailed in the supplementary materials, these values correspond to $EC_{e,saltmax}$= 4 dS m^{-1} and $EC_{e,saltslope}$= 1.3 % per dS m^{-1}. This means that above a soil salinity threshold of about 5.1 mg cm^{-3} (or EC_e= 4 dS m^{-1}), transpiration decreases by 1.03 % for each unit increase in salinity concentration (or 1.3 % per dS m^{-1} increase) with respect to the potential transpiration (Fig. 3). Additionally, the TSCF parameter that represents the uptake of solutes by the roots relative to the uptake of water, is higher than 1, which indicates an active root solute uptake.

Fig. 4 shows the posterior distribution of the calibrated parameters for quinoa under saline conditions in Laayoune and under rainfed conditions in Merelbeke, respectively. The red marker represents the value that best fits the observations, while the blue marker denotes the mean of the prior distribution (initial guess). The range of the x-axis values coincide with the parameter range of variation (Table A.1), except for HLIM3H, HLIM3L, SALTSLOPE and FLTBm in Fig. 4A, and HLIM3H, HLIM3L in Fig. 4B, which have been adjusted for visualization purposes. The posterior distribution shows the parameter variability and uncertainty. In case of ICBA-Q5 under salinity and mild drought stress, the distribution of some parameters, specifically some partitioning parameters FOTBm, FLTBa and FRTBb, extend over the full range of the parameter space. The same pattern occurs for the Belgian case, in almost all partitioning parameters. For the other parameters, the distributions are narrower and tend to cluster around the point of maximum likelihood. In addition, the maximum likelihood value of certain parameters, the one that best fit the observations (indicated by the red marker) does not always correspond with the peak of the distribution. In the Moroccan case, this discrepancy is particularly noticeable for the parameters AMAX, FOTBb, FRTBb, FRTBm, TSCF and RSOIL. In the Belgian case, this occurs for FRTBa, FRTBb and HLIM3H.

3.3. Calibrated model simulations and statistical analysis

3.3.1. Laayoune (Morocco)

Fig. 5 depicts the daily simulated soil salinity concentration over the growing season for the three irrigation salinity levels, and the daily observations from 25 May 2021 onwards. The vertical dashed line marks the start of each irrigation treatment at crop emergence. Before this point, the crop was irrigated with low-salinity water (4 dS m^{-1}). The soil salinity concentration has a peak on mid-May, specifically 11 May, 18 May and 21 May, for the lower, medium and higher salinity levels, respectively, and then gradually decreases until reaching a relatively stable value in all treatments. The simulated peak is higher than the observed one, especially for the medium salinity level of 12 dS m^{-1}.

The cumulative fluxes or water balance components, namely transpiration, evaporation and irrigation, are presented in Fig. 6. Leaching is not shown because it was minimal in this case. The vertical dashed line marks the start of each irrigation treatment at crop emergence. There is a point until which the cumulative evaporation nearly equals cumulative irrigation (around May 10), for all treatments, which aligns approximately with the peaks of soil salinity concentration in Fig. 5. Until this point, most of the irrigation water is lost by soil evaporation. Afterwards, irrigation water is gradually taken by the plant and soil evaporation decreases. The change in water storage during the growing season resulted in −130.1 mm, −127.1 mm and −105.1 mm, for the low, medium and high salinity scenarios, respectively. At high salinity (20 dS m^{-1}), the cumulative transpiration reduction ($T_{pot} - T_{act}$) at the end of the growing season is substantially smaller than the reduction in final T_{pot}, compared to the lower salinity levels. The transpiration reduction represents the stomatal closure caused by salinity and drought stress,

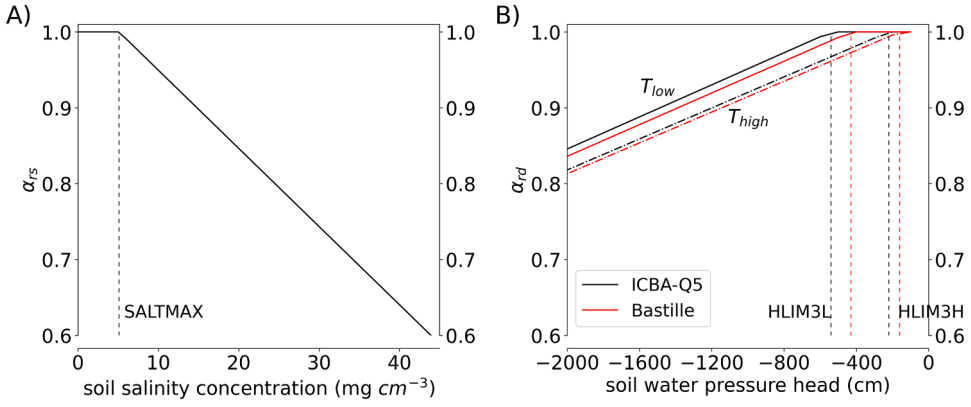

Fig. 3. Transpiration reduction factor due to salinity stress (α_{rs}) as function of soil water salinity concentration (5A), and due to drought stress (α_{rd}) as function of soil water pressure head (5B) for ICBA-Q5 grown in Laayoune, and Bastille in Merelbeke. The dashed vertical lines indicate the different thresholds, SALTMAX, HLIM3L and HLIM3H, that determine the start of transpiration reduction due to stress. SALTMAX is the salinity concentration threshold, and HLIM3L and HLIM3H are the pressure head thresholds for low (T_{low}) or high (T_{high}) atmospheric demand, respectively.

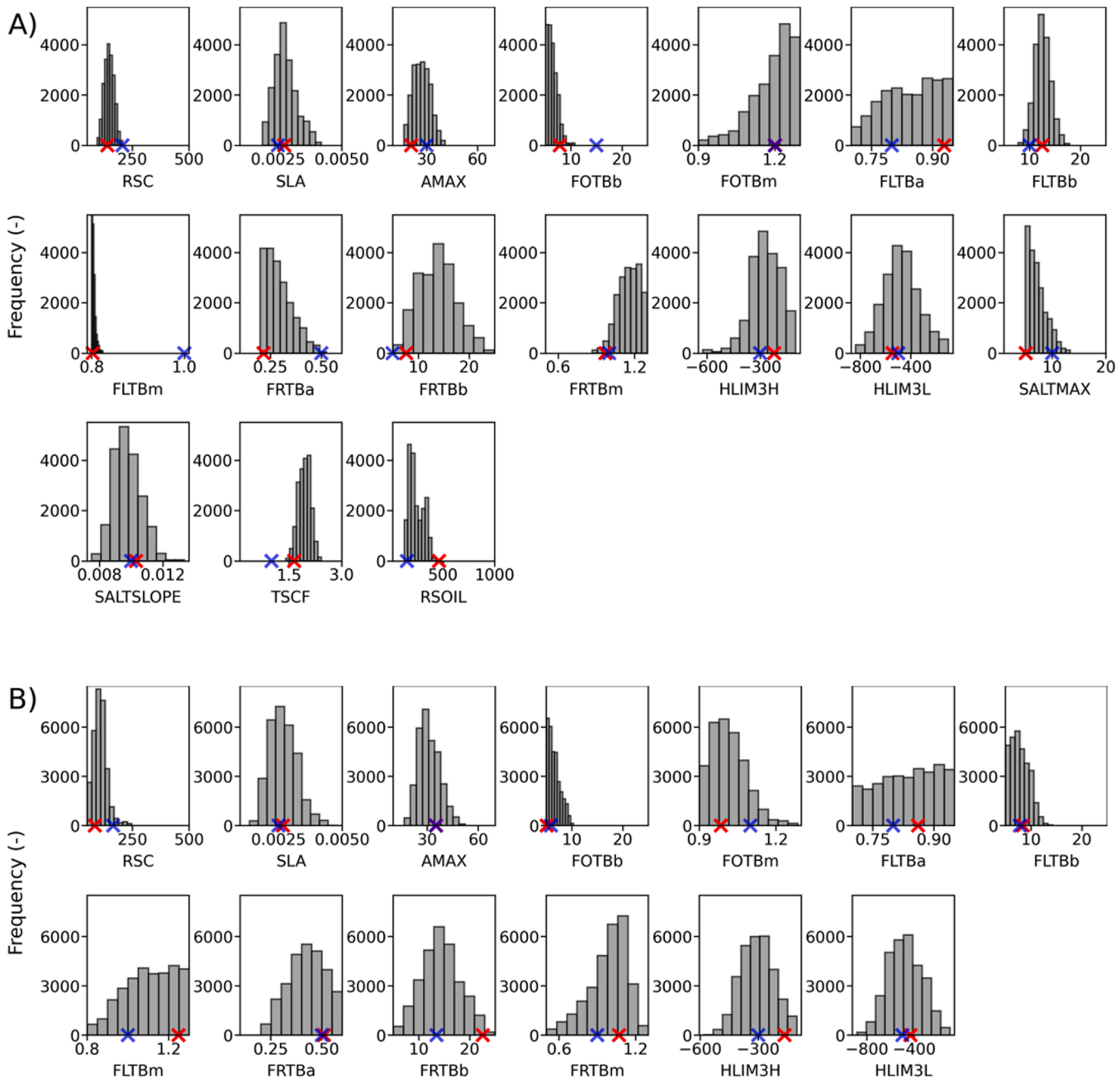

Fig. 4. Parameter distribution as given by DREAMzs, for ICBA-Q5 quinoa variety under saline conditions in Laayoune (Morocco) (6 A) and Bastille under rainfed and non-saline conditions in Merelbeke (Belgium) (6B). The red marker represents the value of the parameter set that best fits the observations, while the blue marker represents the mean of the prior distribution. The range of the x-axis values coincide with the parameter range of variation except for HLIM3H and HLIM3L (A, B), and SALTSLOPE and FLTBm (A), for visualization purposes. The description of the parameters is given in Table A.2 in appendix.

while the reduction in T_{pot} reflects the subsequent decrease in leaf and crop development due to this stomatal closure. As salinity levels increase, salinity stress starts earlier (Fig. B.1 in appendix), which have a greater impact on crop development and transpiration demand.

Fig. 7 shows the daily simulated soil water content over the growing season for the three irrigation salinity levels, and the daily observations from 25 May 2021 onwards. Soil water content is simulated well for the low salinity level, while for the other treatments, the model under- or overestimates the observations, which is particularly evident in the medium salinity treatment.

The observed yield and biomass against the simulated values for the three salinity levels are shown in Fig. 8, together with the 1:1 line that indicates a perfect fit. The relation between yield and biomass reduction with salinity is well approximated at the medium and high salinity levels but is not correctly captured at the low salinity level.

3.3.2. *Merelbeke (Belgium)*

Fig. 9 shows the simulated soil water content over the growing season in 2023 at depths of 0–30 cm, 30–60 cm and 60–90 cm, and the seven average soil moisture observations at each soil depth. The model effectively simulates the soil water content observations, particularly within the top 30 cm of the soil. In the topsoil, the model captures the soil moisture fluctuations due to rainfall events and periods of drought (mid-May – mid-July, 2023), while for the deeper layers, the model overestimates the soil moisture in this dry period. The top layer reached very low moisture levels while the deeper layers retained more soil

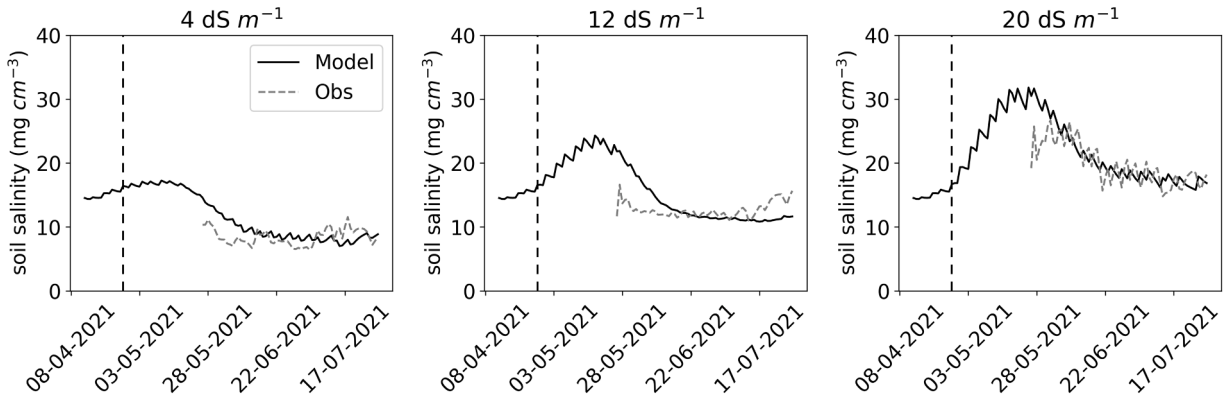

Fig. 5. Observed and simulated soil salinity concentration at 10 cm depth (mg cm^{-3}), for the three irrigation water salinity levels of 4, 12 and 20 dS m^{-1}. Observations start on May 25th, 2021. The vertical dashed line indicates the start of each irrigation treatment, at crop emergence. Before this time, the soil was irrigated with low-salinity water (4 dS m^{-1}).

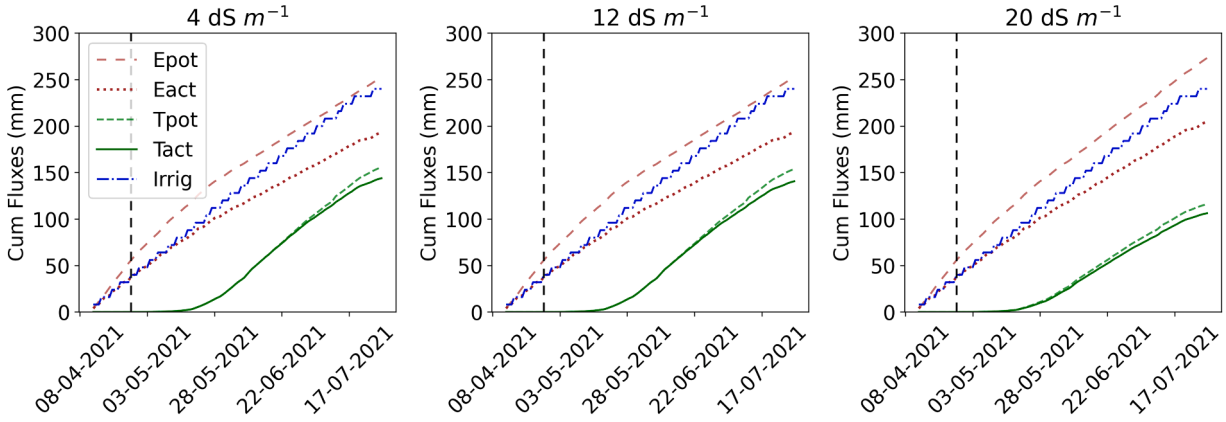

Fig. 6. Simulated cumulative water fluxes for the three irrigation water salinity levels of 4, 12 and 20 dS m^{-1}. Epot and Eact represent potential and actual evaporation, Tpot and Tact denote potential and actual transpiration, and Irrig refers to irrigation. The vertical dashed line indicates the start of each irrigation treatment, at crop emergence. Before this time, the soil was irrigated with low-salinity water (4 dS m^{-1}).

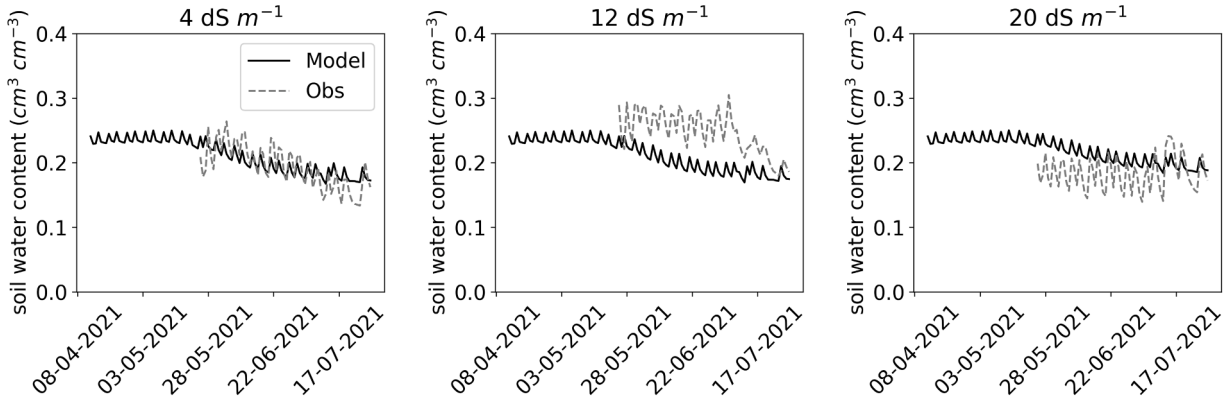

Fig. 7. Observed and simulated soil water content at 10 cm depth (cm^3 cm^{-3}), for the three irrigation water salinity levels of 4, 12 and 20 dS m^{-1}. Observations start on 25 May 2021.

moisture.

Simulated and observed yield, for 2018, 2019, 2022 and 2023 are presented in Fig. 10. Yield in 2022 was significantly higher compared to the other years. On average, the model simulates satisfactorily the yield observations under drought stress (Fig. 10 and Fig. B.2) although with important over- and underestimations. This is partly linked to the presence of diseases that are not included in the model.

Lastly, Fig. 11 shows the simulated Leaf Area Index (LAI, m^2 m^{-2}) during 2023. Eight LAI observations were available during the growing season. The maximum observed LAI is about 4.7, while the simulated maximum value is around 4.1. Overall, the simulated values closely align with the measurements, exhibiting some discrepancies after reaching maximum canopy cover. The decline in the simulated LAI during June and July corresponds to the drought period experienced in 2023.

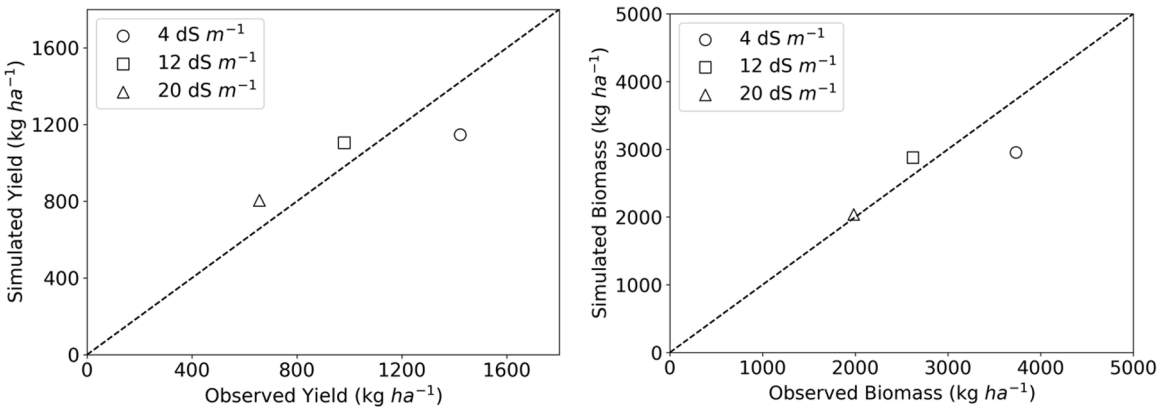

Fig. 8. Observed against simulated yield and biomass (kg ha^{-1}) for the three irrigation water salinity levels of 4, 12 and 20 dS m^{-1}. The black dashed line is the 1:1 line or bisector line that indicates a perfect fit.

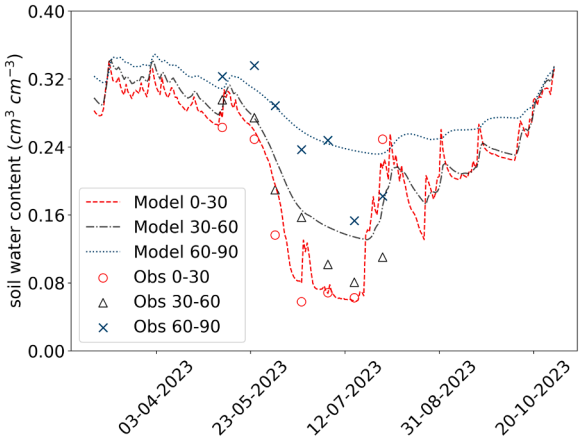

Fig. 9. Observed and simulated soil water content from 0 to 30 cm, 30–60 cm and 60–90 cm depth (cm^3 cm^{-3}), for Bastille during 2023.

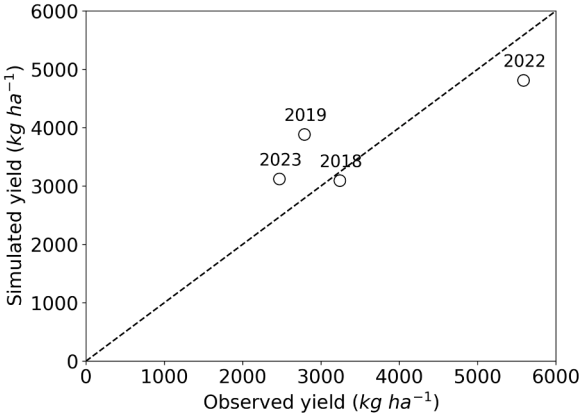

Fig. 10. Observed against simulated yield for 2018, 2019, 2022 and 2023 for Bastille in Merelbeke. The black dashed line is the 1:1 line or bisector line that indicates a perfect fit.

3.3.3. Statistical indices

Table 4 shows the statistical indices Root Mean Square Error (RMSE), Normalized Root Mean Square Error (NRMSE) and coefficient of determination (R^2) for the Moroccan and Belgian cases. These indices give a numerical estimation of how well the model fits the observations, in this case, soil salinity concentration, soil water content, yield, biomass, and LAI. Since these metrics largely summarize the goodness-of-fit of the model in just a number, it is important to always complement them with graphical results that give a broader view of the model performance. The values of RMSE denote high discrepancies for almost all variables. This is the result of few high deviations such as those in yield and biomass at the lowest salinity level, soil salinity peak, soil water content at the medium salinity level and maximum LAI, as detailed in the previous sections. The values of NRMSE are dimensionless and allow comparison between variables. It shows that the simulated soil water content from 60 to 90 cm in Bastille has the lowest relative error, while LAI has the highest relative error, compared to the

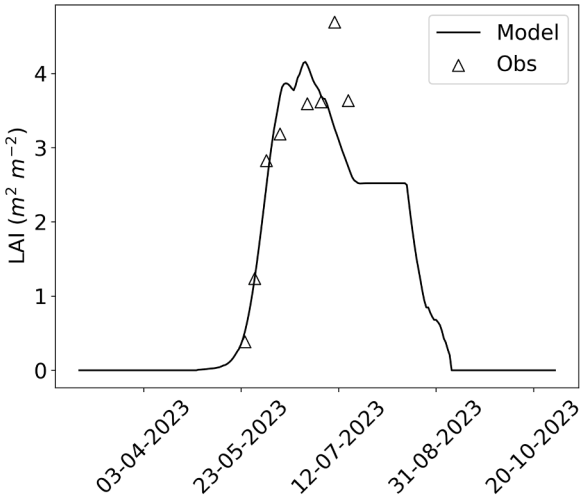

Fig. 11. Simulated and observed Leaf Area Index (LAI, m^2 m^{-2}) for Bastille in 2023.

Table 4
Goodness-of-fit statistics Root Mean Square Error (RMSE), Normalized Root Mean Square Error (NRMSE) and Coefficient of determination (R^2) for all simulated variables, for ICBA-Q5 and Bastille.

Variable	RMSE	NRMSE	R^2	Variety
Soil salinity concentration	3.54 mg cm^{-3}	0.259	0.53	ICBA-Q5
Soil water content	0.04 cm^3 cm^{-3}	0.194	0.03	ICBA-Q5
Yield	194.3 kg ha^{-1}	0.190	0.62	ICBA-Q5
Biomass	475.6 kg ha^{-1}	0.171	0.57	ICBA-Q5
Yield	749.0 kg ha^{-1}	0.213	0.63	Bastille
LAI	0.87 cm^2 cm^{-2}	0.313	0.54	Bastille
Soil water content (0−30)	0.028 cm^3 cm^{-3}	0.179	0.90	Bastille
Soil water content (30–60 cm)	0.038 cm^3 cm^{-3}	0.218	0.76	Bastille
Soil water content (60–90 cm)	0.039 cm^3 cm^{-3}	0.155	0.62	Bastille

mean of the observations. The values of R^2 indicate that overall, at least 50 % of the total variability in the observations is explained by the model, except for soil water content in ICBA-Q5.

4. Discussion

Differences in the calibration between these two varieties are expected (Table A.2 and Fig. 4), especially in the crop parameters for potential transpiration and yield such as TSUMEA, RSC, AMAX, and partitioning coefficients, which are variety dependent (De Wit and Boogaard, 2021; Kroes et al., 2017). ICBA-Q5 was bred to tolerate high levels of salinity, drought, and heat stress in arid regions, whereas Bastille was developed as a disease tolerant variety more suited for temperate climate conditions (longer days and humid environment). ICBA-Q5 has a shorter growing season than Bastille, yet it has a higher temperature requirement for emergence and flowering (TSUMEMEOPT, TSUMEA), indicating its adaptation to hot environments. The parameter RSC, the minimum stomatal resistance, is higher for ICBA-Q5, which gives a lower potential transpiration. This may be an adaptation of ICBA-Q5 to excessive water loss under arid conditions, for example due to a lower stomatal density or regulation of the stomatal closure (Adolf et al., 2013). A modification in the stomatal closure and density also affects how much carbon dioxide (CO_2) is assimilated by the plant. The parameter AMAX, which is the maximum CO_2 assimilation rate, ranges between 30 and 40 kg ha^{-1} h^{-1} for C3 crops (e.g. potato, quinoa, barley, etc) according to De Wit and Boogaard (2021). The value for Bastille falls within this range, whereas ICBA-Q5's value is much lower.

Präger et al. (2019) calibrated several crop parameters under rainfed conditions for the European quinoa varieties Jessie and Zeno, in southwestern Germany, using the CSM-CROPGRO model. Some parameters are transferable to WOFOST parameters, like the specific leaf area (SLA) and partitioning coefficients. For Bastille, SLA, the initial partitioning to the leaves (FLTBa) and the initial partitioning to the roots (FRTBa) are similar to the parameters given by Präger et al. (2019), while for ICBA-Q5, FRTBa is much lower. These parameters, related to potential transpiration and yield, might have implicitly included the effects of drought and salinity stress. Theoretically, stresses should not affect potential production parameters, which are only crop or variety dependent. However, since these parameters were calibrated using data with some sort of stress (drought and salinity stress), they might be slightly affected. This could be one of the reasons why the model falls short in simulating correctly the yield and biomass at the lower salinity level.

The salinity stress parameters for the ICBA-Q5 variety resulted in SALTMAX equal to 5.1 mg cm^{-3} (or $EC_{e,saltmax}$= 4 dS m^{-1}) and SALTSLOPE equal to 0.0103 cm^{-3} mg (or $EC_{e,saltslope}$= 1.3 % per dS m^{-1}), under the arid conditions and salinity levels in the Laayoune region (Fig. 3A). For comparison, conventional arable crops like potato have a SALTMAX of 2.18 mg cm^{-3} and SALTSLOPE of 0.094 cm^{-3} mg, or more tolerant crops like barley have a SALTMAX of 10.24 mg cm^{-3} and SALTSLOPE equal to 0.039 cm^{-3} mg (Kroes et al., 2017). Although quinoa has a lower salinity threshold than barley, quinoa is less affected by increasing salinity. This is in line with the high salinity tolerance reported for quinoa. Another important parameter is TSCF (or K_r in Eq. (2)), which represents the root solute uptake relative to water. One of the reported salinity stress tolerance mechanisms of quinoa is the inclusion of salts in its internal organs (Adolf et al., 2013; Hariadi et al., 2011). The parameter TSCF is larger than 1, indicating an active root solute uptake, which suggests that the ICBA-Q5 variety is a "salt includer". This aligns with the observed rise in Na^+ content in the leaves as salinity increases as shown in El Mouttaqi et al. (2023), and the decrease in soil salinity concentration over the growing season. However, these results contrast with those of a recent study by Comparini et al. (2024), where salt exclusion mechanisms were identified in Vikinga, Dave 407 and Red Head quinoa varieties in a rhizoslides experiment. This underscores the variations in tolerance mechanisms among different varieties and highlights that environmental conditions (i.e. growing on a sheet of paper versus growing in soil) influence the dominating processes in the salt transport pathway.

Theoretically, SALTMAX, SALTSLOPE and TSCF are only able to account for the osmotic adjustment affecting crop transpiration, and salt inclusion mechanisms which influence the amount of solutes present in the soil. Other adaptations observed in quinoa to avoid ion toxicity, like salt storage in external salt glands, are not accounted for in the salinity stress function. Ion toxicity plays an important role at high salinity levels and after long exposure to salinity (Munns and Tester, 2008). Given the capacity of the model to simulate correctly the yield and biomass at high salinity levels (Fig. 8), the salinity stress parameters might incorporate some tolerance mechanisms to avoid ion toxicity. Further research could help to evaluate whether the well-known salinity stress function proposed by Maas and Hoffman (1977) and used in SWAP-WOFOST can indeed indirectly describe ionic effects.

In terms of drought stress parameters, HLIM3H and HLIM3L are similar for both varieties, with ICBA-Q5 resulting in a slightly higher drought tolerance (Fig. 3B), which can be attributed to physiological differences but also to different soil properties and environmental conditions. The calibrated values are in the same range of most arable crops (Kroes et al., 2017; Maas and Hoffman, 1977).

It is important to note that the parameter values presented in Table A.2 are the ones emerging as the 'most likely' ones from the parameter estimation process given the observed data. However, the posterior distribution of these parameters (Fig. 4) shows the complete picture regarding parameter uncertainty. For some parameters, specifically some partitioning parameters such as FOTBm, FLTBa and FRTBb, we see that the distribution extends over the full range of the parameter space, for both case studies. In case of non-sensitive parameters like FLTBa and FRTBb, it is expected that they exhibit a more uniform distribution because variations in their values do not significantly affect the model output. However, this does not occur for other non-sensitive parameters such us HLIM3H and HLIM3L, which have a narrow distribution. This is because they may be influential for soil water content, which was not included in the sensitivity analysis. On the other hand, for sensitive parameters such as FOTBm, the widespread distribution shows that the available data is insufficient to narrow down to its exact value. This is reasonable because the partitioning coefficients vary with the development stage of the crop, and we only had observations of the final yield and biomass. This also stresses the importance of time series data for crop model calibration (Coudron et al., 2021). In addition, the maximum likelihood value, denoted with a red marker, does not always correspond with the peak of the distribution. This discrepancy is commonly seen in multi-dimensional problems, where the probability mass of a given distribution tends to spread out further from the point of maximum likelihood (Carpenter, 2017).

The simulated soil salinity concentration, soil water content, yield, and biomass show overall good agreement with the observations in Laayoune. It was shown that during the vegetative period, the model tends to accumulate more solutes in the soil than observed, but later it gets closer to the observations (Fig. 5). The simulated salt accumulation during the germination and seedling stage is largely influenced by the high soil evaporation (Fig. 6), which mostly depends on the soil hydraulic properties of the surface layer. It is possible that with different soil parameter values, greater leaching might occur, reducing salt concentration in the top soil layer. Since measurements were only available from 25 May 2021 onward, we were unable to verify the soil salinity simulation before this date. The model simulated the overall trends and fluctuations in the soil water content caused by root water uptake and irrigation events, although some deviations were observed, particularly at the 12 dS m^{-1} experiment (Fig. 7). Several factors might contribute to these deviations: unknown initial soil moisture conditions, spatial soil heterogeneity, uncalibrated soil parameters and sensor measurement uncertainty.

During the germination and seedling stage, most of the irrigation

water is lost by evaporation (Fig. 6), while the salts remain in the topsoil layer. As the crop develops, evaporation decreases while transpiration increases, leading to a reduction in soil salinity since the crop actively takes up salts. Under high salinity levels (20 dS m^{-1}), the potential transpiration is much smaller than for the lower salinity levels (4 dS m^{-1} and 12 dS m^{-1}), yet the transpiration reduction is very similar across salinity treatments (Fig. 6). This highlights the dominant impact of salinity on reducing biomass and leaf area, which in turn reduces the potential of the crop to transpire. The similar transpiration reduction among treatments indicates a "compensation" effect. Under low and medium salinity stress, the crop growth was inhibited by drought stress due to insufficient water, as all treatments received the same irrigation amount. In contrast, at higher salinity levels, the crop growth was limited primarily by salinity stress rather than drought stress, since the crop water requirements were lower (Fig. B.1 in appendix).

The effect of salinity stress is evident in the decreased crop transpiration and yield, although this effect is not well captured at the low salinity level (Fig. 8). However, even at high salinity levels, ICBA-Q5 is still able to grow and give significant yields. These findings suggest that selecting varieties with higher drought and salinity tolerance, such as ICBA-Q5, could improve crop resilience in arid regions. Additionally, crop management practices aimed at reducing excessive soil evaporation and consequent salt accumulation, especially during germination and seedling stages, such as improved irrigation planning or mulching, would be highly beneficial.

Under Northwestern European conditions (Merelbeke, Belgium), the model effectively replicated the impacts of drought stress over the years on transpiration (Fig. B.2), yield (Fig. 10) and LAI (Fig. 11), although it cannot incorporate situations involving weeds and diseases, which are prevalent in this climatic condition. The observed yield in 2022 was high compared to the other years, since quinoa was planted earlier. Early planting proved advantageous as it allowed the plants to reach a sufficient size by the time pests could proliferate, and the relatively dry year further minimized pest problems. Quinoa is very susceptible to weeds and diseases in wet years, and the yield is highly dependent of these factors. This is a limitation in most crop models including SWAP-WOFOST that only account for abiotic stresses (suboptimal soil moisture, salinity or temperature).

In Belgium, soil salinization is currently not a major problem in most agricultural areas. However, groundwater salinization in areas influenced by the sea (i.e. polders), or the use of treated wastewater for irrigation, may become more common due to more frequent droughts and freshwater scarcity in the future. Currently, Belgian farmers do not irrigate quinoa, and some small-scale production is found in the polder area (e.g. Belgische Quinoa). Developing a model that accounts for salinity stress is the first step for evaluating quinoa performance under future salinization scenarios in this region, using for example, the salinity stress parameters of ICBA-Q5 as an approximation.

5. Conclusion

The objective of this study was to calibrate the crop growth, solute transport and salinity and drought stress parameters of the SWAP – WOFOST model, and to investigate whether this model could represent the stress tolerance mechanisms observed in quinoa, especially to salinity. The simple salinity stress function proved effective in simulating the salinity tolerance mechanisms of quinoa under the hot-arid climate of Laayoune, Morocco, and transferring these effects to transpiration and yield. However, at low salinity levels, the model did not accurately capture the relation between yield and salinity. The parametrization of the model implied that the ICBA-Q5 quinoa variety is a "salt includer", which aligns with the observed rise in Na^+ content in the leaves as salinity increases, and the decrease in soil salinity concentration over the growing season. Our work confirmed that the current approach to represent salt stress in the model, can also be used to represent crops that take up salts and develop mechanisms to deal with high uptake of salts, like some halophytes. The model results also showed that high soil evaporation at the start of the growing season is an important factor driving salt accumulation in the soil, thereby intensifying salinity stress in the arid region of Laayoune. In the Northwestern European climate of Merelbeke, Belgium, the model effectively simulated the impact of drought stress on LAI and yield of the Bastille variety. Future research could use these calibrated models to evaluate management practices such as improved irrigation strategies and mulching to reduce evaporation and salt accumulation in arid conditions, and to analyze quinoa performance under potential droughts or future salinization in Northwestern European conditions. Thanks to our Bayesian parameter inference approach, we obtained uncertainty distributions on the estimated parameters. However, to reduce this uncertainty and extend the applicability of the calibrated models to conditions beyond those analyzed in this study, additional local experimental data is necessary.

Funding

This research was part of the SALAD (Saline AgricuLture for ADaptation) project. This project is part of the programme of the ERA-NET Cofund FOSC that received funding from the European Union's Horizon 2020 research and innovation programme under grant agreement No 862555.

CRediT authorship contribution statement

Estrella Delgado Diana Catalina: Writing – original draft, Visualization, Software, Methodology, Investigation, Formal analysis, Data curation, Conceptualization. **De Swaef Tom:** Writing – review & editing, Supervision, Methodology, Conceptualization. **Vanderborght Jan:** Writing – review & editing, Supervision, Methodology, Conceptualization. **Laloy Eric:** Software, Resources. **Cnops Gerda:** Writing – review & editing, Investigation. **De Boever Maarten:** Writing – review & editing, Investigation. **Hirich Abdelaziz:** Writing – review & editing, Investigation. **El Mouttaqi Ayoub:** Investigation. **Garré Sarah:** Writing – review & editing, Supervision, Project administration, Methodology, Funding acquisition, Conceptualization.

Declaration of Competing Interest

The authors declare that they have no known competing financial interests or personal relationships that could have appeared to influence the work reported in this paper.

Acknowledgements

We would like to thank our partners from the SALAD project for their collaboration throughout this project. We also extend our thanks to the funders for their support, which made this research possible. Finally, we thank the reviewers for their constructive feedback which helped to improve the manuscript.

Supplementary materials

The following supplementary materials for this article can be found online: Procedure to convert saturated past extract (ECe) to soil salinity concentration (c). Calibration of WOFOST tabular parameters using logistic functions. Fig. S.1. Summary statistics of Morris method on yield, biomass, actual transpiration and root solute uptake, for the Moroccan case, under low (4 dS m^{-1}), medium (12 dS m^{-1}), and high (20 dS m^{-1}) irrigation salinity water. Fig. S.2. Summary statistics of Morris method on yield, biomass and actual transpiration, for the Belgian case, averaged over the years 2018, 2019, 2022 and 2023.

Appendix A. Crop and solute transport parameters

Table A.1
Crop and solute transport parameters for quinoa considered for sensitivity analysis. Parameter ranges are based on De Wit and Boogaard (2021) and available information within crop and swap files, and adjusted according to observed data

Parameter	Range of variation	Units	Description
TSUMEMEOPT	50–200	°C	Temperature sum from sowing to emergence
TSUMEA	150–1050	°C	Temperature sum from emergence to anthesis
TSUMAM	600–1550	°C	Temperature sum from anthesis to maturity
RSC	50–500	s m^{-1}	Minimum canopy resistance (stomatal resistance)
TDWI	0.5–500	kg ha^{-1}	Initial total crop dry weight
RGRLAI	0.007–0.5	m^2 m^{-2} day^{-1}	Maximum relative increase in LAI
SPAN	17–50	day	Life span of leaves under optimum conditions
KDIF	0.44–1.0		Extinction coefficient for diffuse visible light
SLA	0.001–0.005	ha kg^{-1}	Specific leaf area as function of crop development
AMAX	10–70	kg ha^{-1} h^{-1}	CO2 assimilation rate as function of development stage
CVO	0.45–0.7	-	Efficiency of conversion into storage organs
Q10	1.5–2.0	-	Increase in respiration rate per 10°C temperature change
RMO	0.002–0.03	kg(CH_2O) kg^{-1} day^{-1}	Relative maintenance respiration rate of storage organs
FRTBa	0.2–0.7	-	Parameters of the logistic function that describe the fraction of total dry matter increase partitioned to the roots. *a* refers to allocation at emergence, *b* the steepness of the function and *m* the location of the centre point (See supplementary materials)
FRTBb	5–25		
FRTBm	0.5–1.3		
FLTBa	0.7–0.95	-	Parameters of the logistic function that describe the fraction of total above ground dry matter increase partitioned to the leaves
FLTBb	5–25		
FLTBm	0.8–1.3		
FOTBb	5–25	-	Parameters of the logistic function that describe the fraction of total above ground dry matter increase partitioned to the storage organs
FOTBm	0.9–1.3		
RDI	5–20	cm	Initial rooting depth
RDC	10–50	cm	Maximum rooting depth
RRI	0.00001–3.0	cm day^{-1}	Maximum daily increase in rooting depth
HLIM3H	−10000 - −100	-	Pressure head below which water uptake reduction starts at high potential transpiration
HLIM3L	−10000 - −100	-	Pressure head below which water uptake reduction starts at low potential transpiration
SALTMAX	1–20	mg cm^{-3}	Threshold of salt concentration in soil water
SALTSLOPE	0.0005–0.1	cm^3 mg^{-1}	Decline of root water uptake above threshold
TSCF	0.1–3.0	-	Relative uptake of solutes by roots
RSOIL	10–1000	s m^{-1}	Soil resistance of a wet soil

Table A.2
Calibrated and estimated crop and solute transport parameters for quinoa ICBA-Q5 under Moroccan (MO) conditions and Bastille under Belgian (BE) conditions. The calibrated values represent the value with maximum likelihood

Parameters	Value MO	Value BE	Units	Description	Remarks
TSUMEMEOPT	170	80	°C	Temperature sum from sowing to emergence	Estimated from weather data
TSUMEA	715	450	°C	Temperature sum from emergence to anthesis	Estimated from weather data
TSUMAM	1100	1100	°C	Temperature sum from anthesis to maturity	Estimated from weather data
TBASEM	2	2	°C	Minimum temperature, used for germination trajectory	AquaCrop quinoa file
TEFFMX	30	30	°C	Maximum temperature, used for germination trajectory	AquaCrop quinoa file
ALBEDO	0.19	0.19		Crop reflection factor	WOFOST potato crop file
RSC	140	85	s m^{-1}	Minimum canopy resistance (stomatal resistance)	Calibrated
TDWI	1.0	5.0	kg ha^{-1}	Initial total crop dry weight	Estimated from data, taking into account emergence rate
LAIEM	0.05	0.05		Leaf area index at emergence	Based on Präger et al. (2019)
RGRLAI	0.09	0.09	m^2 m^{-2} day^{-1}	Maximum relative increase in LAI	Estimated from data
SPAN	37	37	day	Life span of leaves under optimum conditions	WOFOST potato crop file
SLA	0.0027	0.0027	ha kg^{-1}	Specific leaf area as function of crop development	Calibrated
KDIF	0.85	0.85		Extinction coefficient for diffuse visible light	Adjusted based on Kroes et al. (2017)
KDIR	0.75	0.75		Extinction coefficient for direct visible light	
AMAX	20.9	35.2	kg ha^{-1} h^{-1}	Maximum CO2 assimilation rate as function of development stage	Calibrated
CVL	0.72	0.72		Efficiency of conversion into leaves	WOFOST potato crop file
CVO	0.50	0.50		Efficiency of conversion into storage organs	Estimate for high protein crops (Wit & Boogaard, 2021)

(*continued on next page*)

Table A.2 (*continued*)

Parameters	Value MO	Value BE	Units	Description	Remarks
CVR	0.72	0.72		Efficiency of conversion into roots	WOFOST potato crop file
CVS	0.69	0.69		Efficiency of conversion into stems	WOFOST potato crop file
Q10	2.0	2.0		Increase in respiration rate per 10°C temperature change	WOFOST potato crop file
RML	0.030	0.030	$kg(CH_2O)$ kg^{-1} day^{-1}	Relative maintenance respiration rate of leaves	WOFOST potato crop file
RMO	0.010	0.010	$kg(CH_2O)$ kg^{-1} day^{-1}	Relative maintenance respiration rate of storage organs	WOFOST barley crop file
RMR	0.010	0.010	$kg(CH_2O)$ kg^{-1} day^{-1}	Relative maintenance respiration rate of roots	WOFOST potato crop file
RMS	0.015	0.015	$kg(CH_2O)$ kg^{-1} day^{-1}	Relative maintenance respiration rate of stems	WOFOST potato crop file
FRTBa	0.22	0.51		Parameters of the logistic function that describe the fraction of total dry matter increase partitioned to the roots. *a* refers to allocation at emergence, *b* the steepness of the function and *m* the location of the centre point (See supplementary materials)	Calibrated
FRTBb	7.695	22.56			
FRTBm	0.97	1.07			
FLTBa	0.93	0.86		Parameters of the logistic function that describe the fraction of total above ground dry matter increase partitioned to the leaves	Calibrated
FLTBb	12.57	8.43			
FLTBm	0.80	1.25			
FOTBb	7.85	5.07			
FOTBm	1.20	0.984		Parameters of the logistic function that describe the fraction of total above ground dry matter increase partitioned to the storage organs	Calibrated
RDI	10.0	10.0	cm	Initial rooting depth	WOFOST potato crop file
RDC	20.0	25.0	cm	Maximum rooting depth	Estimated from data
RRI	1.2	1.2	cm day^{-1}	Maximum daily increase in rooting depth	WOFOST potato crop file
HLIM3H	−220	−160	cm	Pressure head below which water uptake reduction starts at high potential transpiration	Calibrated
HLIM3L	−540	−430	cm	Pressure head below which water uptake reduction starts at low potential transpiration	Calibrated
SALTMAX	5.1		mg cm^{-3}	Threshold of salt concentration in soil water	Calibrated for Morocco
SALTSLOPE	0.0103		cm^3 mg^{-1}	Decline of root water uptake above threshold	Calibrated for Morocco
TSCF	1.64			Relative uptake of solutes by roots	Calibrated for Morocco
RSOIL	460	150	s m^{-1}	Soil resistance of a wet soil	Calibrated for Morocco

Appendix B. : Transpiration reduction due to drought and salinity stress

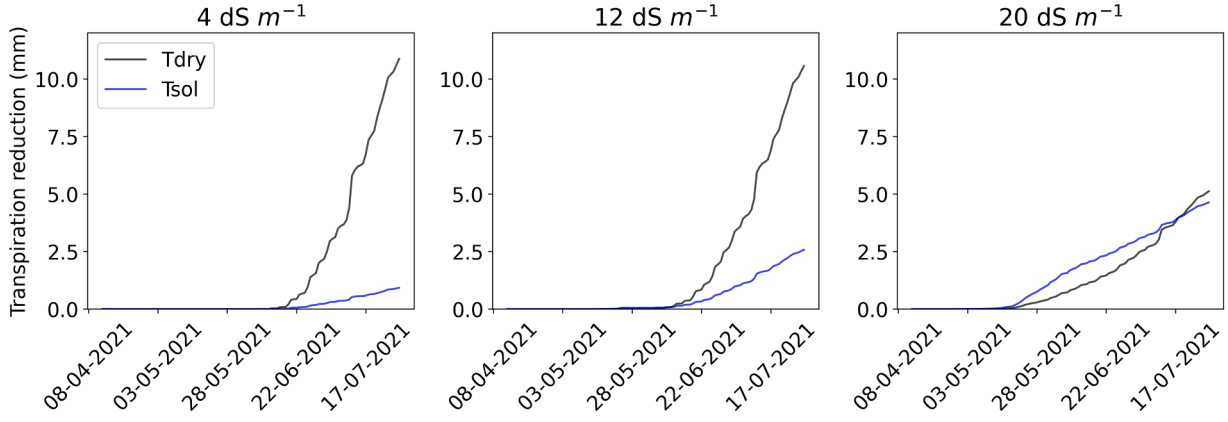

Fig. B.1. Cumulative transpiration reduction due to salinity (Tsol) and drought (Tdry) stress for ICBA-Q5 in Laayoune, for the three irrigation water salinity levels of 4, 12 and 20 dS m^{-1}

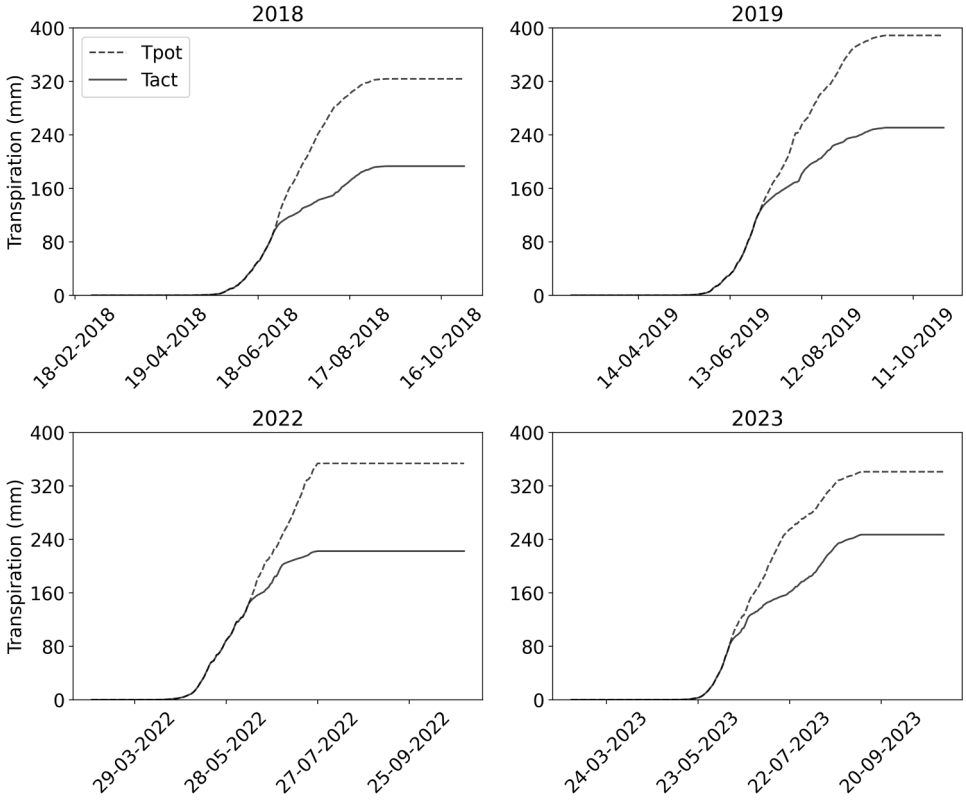

Fig. B.2. Cumulative potential and actual transpiration for Bastille in Merelbeke, for 2018, 2019, 2022 and 2023

Appendix C. Supporting information

Supplementary data associated with this article can be found in the online version at doi:10.1016/j.agwat.2025.109356.

Data availability

The data used for model calibration and the python scripts for model execution and sensitivity analysis are open access and are available in https://doi.org/10.5281/zenodo.14163468 and https://gitlab.ilvo.be/plant-modelling/swap-dream. The python version of the DREAMzs algorithm used in this study can be obtained upon request.

References

Adolf, V.I., Shabala, S., Andersen, M.N., Razzaghi, F., Jacobsen, S.-E., 2012. Varietal differences of quinoa's tolerance to saline conditions. Plant Soil 357, 117–129. https://doi.org/10.1007/s11104-012-1133-7.

Adolf, V.I., Jacobsen, S.-E., Shabala, S., 2013. Salt tolerance mechanisms in quinoa (Chenopodium quinoa Willd.). Environ. Exp. Bot. 92, 43–54. https://doi.org/10.1016/j.envexpbot.2012.07.004. Sustainable cultivation and exploitation of halophyte crops in a salinizing world.

Alvar-Beltrán, J., Gobin, A., Orlandini, S., Dalla Marta, A., 2020. AquaCrop parametrisation for quinoa in arid environments. Ital. J. Agron. 16. https://doi.org/10.4081/ija.2020.1749.

Arora, S., Dagar, J.C., 2019. Salinity tolerance indicators. In: Dagar, Jagdish Chander, Yadav, R.K., Sharma, P.C. (Eds.), Research Developments in Saline Agriculture. Springer, Singapore, pp. 155–201. https://doi.org/10.1007/978-981-13-5832-6_5.

Atzori, G., 2021. The Potential of Edible Halophytes as New Crops in Saline Agriculture: The Ice Plant (Mesembryanthemum crystallinum L.) Case Study, in: Future of Sustainable Agriculture in Saline Environments. CRC Press.

Bidalia, A., Vikram, K., Yamal, G., Rao, K.S., 2019. Effect of salinity on soil nutrients and plant health. In: Akhtar, M.S. (Ed.), Salt Stress, Microbes, and Plant Interactions: Causes and Solution, 1. Springer, Singapore, pp. 273–297. https://doi.org/10.1007/978-981-13-8801-9_13.

Boesten, J.J.T.I., Stroosnijder, L., 1986. Simple model for daily evaporation from fallow tilled soil under spring conditions in a temperate climate. NJAS 34, 75–90. https://doi.org/10.18174/njas.v34i1.16818.

Bouras, H., Choukr-Allah, R., Amouaouch, Y., Bouaziz, A., Devkota, K.P., El Mouttaqi, A., Bouazzama, B., Hirich, A., 2022. How does quinoa (Chenopodium quinoa Willd.) respond to phosphorus fertilization and irrigation water salinity? Plants 11, 216. https://doi.org/10.3390/plants11020216.

ter Braak, C.J.F., Vrugt, J.A., 2008. Differential evolution markov chain with snooker updater and fewer chains. Stat. Comput. 18, 435–446. https://doi.org/10.1007/s11222-008-9104-9.

Comparini, D., Mozzo, G., Thiers, L., Vanderborght, J., De Swaef, T., Mancuso, S., Garré, S., Atzori, G., 2024. Exploring tolerance mechanisms and root morphological development of New Zealand spinach and quinoa across salinity levels. South Afr. J. Bot. 171, 10–20. https://doi.org/10.1016/j.sajb.2024.05.050.

Coudron, W., Gobin, A., Boeckaert, C., De Cuypere, T., Lootens, P., Pollet, S., Verheyen, K., De Frenne, P., De Swaef, T., 2021. Data collection design for calibration of crop models using practical identifiability analysis. Comput. Electron. Agric. 190, 106457. https://doi.org/10.1016/j.compag.2021.106457.

Dalton, F.N., Raats, P. a C., Gardner, W.R., 1975. Simultaneous uptake of water and solutes by plant roots. Agron. J. 67, 334–339. https://doi.org/10.2134/agronj1975.00021962006700030013x.

De Bock, P., Van Bockstaele, F., Muylle, H., Quataert, P., Vermeir, P., Eeckhout, M., Cnops, G., 2021. Yield and nutritional characterization of thirteen quinoa (Chenopodium quinoa Willd.) varieties grown in North-West Europe—Part I. Plants 10, 2689. https://doi.org/10.3390/plants10122689.

De Bock, P., Cnops, G., Muylle, H., Quataert, P., Eeckhout, M., Van Bockstaele, F., 2022. Physicochemical characterization of thirteen quinoa (Chenopodium quinoa Willd.) varieties grown in North-West Europe—Part II. Plants 11, 265. https://doi.org/10.3390/plants11030265.

De Jong van Lier, Q., van Dam, J.C., Metselaar, K., 2009. Root water extraction under combined water and osmotic stress. Soil Sci. Soc. Am. J. 73, 862–875. https://doi.org/10.2136/sssaj2008.0157.

De Wit, A., Boogaard, H., 2021. A Gentle Introduction to WOFOST.

De Wit, A., Wolf, J., 2010. Calibration of WOFOST Crop Growth Simulation Model for Use within CGMS.

De Wit, A., Boogaard, H.L., Supit, I., Van Den Berg, M., 2020. System Description of the WOFOST 7.2, Cropping Systems Model.

El Mouttaqi, A., Sabraoui, T., Belcaid, M., Ibourki, M., Mnaouer, I., Lazaar, K., Sehbaoui, F., Ait Elhaj, R., Khaldi, M., Rafik, S., Zim, J., Nilahyane, A., Ghoulam, C.,

Devkota, K.P., Kouisni, L., Hirich, A., 2023. Agro-morphological and biochemical responses of quinoa (Chenopodium quinoa Willd. var: ICBA-Q5) to organic amendments under various salinity conditions. Front. Plant Sci. 14, 1143170. https://doi.org/10.3389/fpls.2023.1143170.

FAO, 2021. World Soil Day: FAO highlights the threat of soil salinization to global food security [WWW Document]. Newsroom. URL ⟨https://www.fao.org/newsroom/detail/world-soil-day-fao-highlights-threat-of-soil-salinization-to-food-security-031221/en⟩ (Accessed 5.24.24).

Feddes, R.A., Kowalik, P.J., Zaradny, H., 1978. Simulation of field water use and crop yield, Simulation monographs. Centre for Agricultural Publishing, Wageningen.

Geerts, S., Raes, D., Garcia, M., Miranda, R., Cusicanqui, J.A., Taboada, C., Mendoza, J., Huanca, R., Mamani, A., Condori, O., Mamani, J., Morales, B., Osco, V., Steduto, P., 2009. Simulating yield response of quinoa to water availability with AquaCrop. Agron. J. 101, 499–508. https://doi.org/10.2134/agronj2008.0137s.

Gelman, A., Rubin, D.B., 1992. Inference from iterative simulation using multiple sequences. Stat. Sci. 7. https://doi.org/10.1214/ss/1177011136.

Gould, I., De Waegemaeker, J., Tzemi, D., Wright, I., Pearson, S., Ruto, E., Karrasch, L., Christensen, L.S., Aronsson, H., Eich-Greatorex, S., Bosworth, G., Vellinga, P., 2021. Salinization threats to agriculture across the North Sea Region. Future of Sustainable Agriculture in Saline Environments. CRC Press, Boca Raton, pp. 71–92. https://doi.org/10.1201/9781003112327-5.

Hariadi, Y., Marandon, K., Tian, Y., Jacobsen, S.-E., Shabala, S., 2011. Ionic and osmotic relations in quinoa (Chenopodium quinoa Willd.) plants grown at various salinity levels. J. Exp. Bot. 62, 185–193. https://doi.org/10.1093/jxb/erq257.

Heinen, M., Mulder, M., Van Dam, J., Bartholomeus, R., De Jong Van Lier, Q., De Wit, J., De Wit, A., Hack - Ten Broeke, M., 2024. SWAP 50 years: advances in modelling soil-water-atmosphere-plant interactions. Agric. Water Manag. 298, 108883. https://doi.org/10.1016/j.agwat.2024.108883.

Herman, J., Usher, W., 2017. SALib: an open-source python library for sensitivity analysis. JOSS 2, 97. https://doi.org/10.21105/joss.00097.

Hinojosa, L., Gonz\' alez, J., Barrios-Masias, F., Fuentes, F., Murphy, K., 2018. Quinoa abiotic stress responses: a review. Plants 7, 106. https://doi.org/10.3390/plants7040106.

Hirich, A., Rafik, S., Rahmani, M., Fetouab, A., Azaykou, F., Filali, K., Ahmadzai, H., Jnaoui, Y., Soulaimani, A., Moussafir, M., El Gharous, M., Karboune, S., Sbai, A., Choukr-Allah, R., 2021. Development of quinoa value chain to improve food and nutritional security in rural communities in rehamna, morocco: lessons learned and perspectives. Plants 10, 301. https://doi.org/10.3390/plants10020301.

ILVO, 2023. Quinoa Lokaal [WWW Document]. URL ⟨https://www.quinoalokaal.be/nl/⟩ (Accessed 7.3.24).

Ince Kaya, Ç., Yazar, A., 2016. Saltmed model performance for quinoa irrigated with fresh and saline water in a mediterranean environment. Irrig. Drain. 65, 29–37. https://doi.org/10.1002/ird.1951.

Iwanaga, T., Usher, W., Herman, J., 2022. Toward SALib 2.0: advancing the accessibility and interpretability of global sensitivity analyses. SESMO 4, 18155. https://doi.org/10.18174/sesmo.18155.

Jacobsen, S. -E., 2017. The scope for adaptation of quinoa in Northern Latitudes of Europe. J. Agron. Crop Sci. 203, 603–613. https://doi.org/10.1111/jac.12228.

Jaramillo Roman, V., van de Zedde, R., Peller, J., Visser, R.G.F., van der Linden, C.G., van Loo, E.N., 2021. High-resolution analysis of growth and transpiration of quinoa under saline conditions. Front. Plant Sci. 12. https://doi.org/10.3389/fpls.2021.634311.

Jarvis, N.J., 1989. A simple empirical model of root water uptake. J. Hydrol. 107, 57–72. https://doi.org/10.1016/0022-1694(89)90050-4.

Jarvis, N.J., 2011. Simple physics-based models of compensatory plant water uptake: concepts and eco-hydrological consequences. Hydrol. Earth Syst. Sci. 15, 3431–3446. https://doi.org/10.5194/hess-15-3431-2011.

Kiani-Pouya, A., Rasouli, F., Shabala, L., Tahir, A.T., Zhou, M., Shabala, S., 2020. Understanding the role of root-related traits in salinity tolerance of quinoa accessions with contrasting epidermal bladder cell patterning. Planta 251, 103. https://doi.org/10.1007/s00425-020-03395-1.

Koyro, H.-W., Eisa, S.S., 2008. Effect of salinity on composition, viability and germination of seeds of Chenopodium quinoa Willd. Plant Soil 302, 79–90. https://doi.org/10.1007/s11104-007-9457-4.

Kroes, J.G., Dam, J.C., Bartholomeus, R.P., Groenendijk, P., Heinen, M., Hendriks, R.F.A., Mulder, H.M., Supit, I., Van Walsum, P.E.V., 2017. Swap version 4: Theory description and user manual (techreport). Wageningen Environmental Research, Wageningen.

Laloy, E., Vrugt, J.A., 2012. Highdimensional posterior exploration of hydrologic models using multipletry DREAM(ZS) and highperformance computing. Water Resour. Res. 48. https://doi.org/10.1029/2011wr010608.

Lavini, A., Pulvento, C., d'Andria, R., Riccardi, M., Choukr-Allah, R., Belhabib, O., Yazar, A., İncekaya, Ç., Metin Sezen, S., Qadir, M., Jacobsen, S. -E., 2014. Quinoa's potential in the mediterranean region. J. Agron. Crop Sci. 200, 344–360. https://doi.org/10.1111/jac.12069.

Maas, E.V., Hoffman, G.J., 1977. Crop salt tolerance—current assessment. J. Irrig. Drain. Div. 103, 115–134. https://doi.org/10.1061/jrcea4.0001137.

Meter, 2018. Soil Electrical Conductivity: A Beginner's Guide to Measurements.

Misle, E., Kahlaoui, B., 2015. Nonlinear allometric equation for crop response to soil salinity. J. Stress Physiol. Biochem. 11, 49.

Moog, M.W., Trinh, M.D.L., Nørrevang, A.F., Bendtsen, A.K., Wang, C., Østerberg, J.T., Shabala, S., Hedrich, R., Wendt, T., Palmgren, M., 2022. The *epidermal bladder cell-free* mutant of the salt-tolerant quinoa challenges our understanding of halophyte crop salinity tolerance. N. Phytol. 236, 1409–1421. https://doi.org/10.1111/nph.18420.

Morris, M.D., 1991. Factorial sampling plans for preliminary computational experiments. Technometrics 33, 161–174. https://doi.org/10.1080/00401706.1991.10484804.

Mualem, Y., 1976. A new model for predicting the hydraulic conductivity of unsaturated porous media. Water Resour. Res. 12, 513–522. https://doi.org/10.1029/WR012i003p00513.

Munns, R., Tester, M., 2008. Mechanisms of salinity tolerance. Annu. Rev. Plant Biol. 59, 651–681. https://doi.org/10.1146/annurev.arplant.59.032607.092911.

Nanduri, K.R., Hirich, A., Salehi, M., Saadat, S., Jacobsen, S.E., 2019. Quinoa: a new crop for harsh environments. In: Gul, B., Böer, B., Khan, M.A., Clüsener-Godt, M., Hameed, A. (Eds.), Sabkha Ecosystems, Tasks for Vegetation Science. Springer International Publishing, Cham, pp. 301–333. https://doi.org/10.1007/978-3-030-04417-6_19.

Negacz, K., Vellinga, P., Barrett-Lennard, E., Choukr-Allah, R., Elzenga, T., 2021. Future of Sustainable Agriculture in Saline Environments, 1st ed. CRC Press, Boca Raton. https://doi.org/10.1201/9781003112327.

Peyghan, K., Golabi, M., Albaji, M., 2020. Simulation of quinoa (*Chenopodium* quinoa) yield and soil salinity under salinity and water stress using the SALTMED model. Commun. Soil Sci. Plant Anal. 51, 2361–2376. https://doi.org/10.1080/00103624.2020.1836203.

Präger, A., Boote, K.J., Munz, S., Graeff-Hönninger, S., 2019. Simulating growth and development processes of quinoa (Chenopodium quinoa Willd.): adaptation and evaluation of the CSM-CROPGRO model. Agronomy 9, 832. https://doi.org/10.3390/agronomy9120832.

Pulvento, C., Riccardi, M., Lavini, A., D'Andria, R., Iafelice, G., Marconi, E., 2010. Field trial evaluation of two chenopodium quinoa genotypes grown under rain-fed conditions in a typical mediterranean environment in South Italy. J. Agron. Crop Sci. 196, 407–411. https://doi.org/10.1111/j.1439-037X.2010.00431.x.

Pulvento, C., Riccardi, M., Lavini, A., D'andria, R., Ragab, R., 2013. Saltmed model to simulate yield and dry matter for quinoa crop and soil moisture content under different irrigation strategies in South Italy. Irrig. Drain. 62, 229–238. https://doi.org/10.1002/ird.1727.

Raes, D., Steduto, P., Hsiao, T.C., Fereres, E., 2023a. Reference Manual, Chapter 3 – AquaCrop, Version 7.1. FAO 178.

Raes, D., Steduto, P., Hsiao, T.C., Fereres, E., 2023b. Reference Manual, Chapter 2 – AquaCrop, Version 7.1. FAO, Rome.

Rafik, S., Rahmani, M., Choukr-Allah, R., El Gharous, M., Calle, J.P.R., Filali, K., Hirich, A., 2021. Techno-economic assessment of quinoa production and transformation in Morocco. Environ. Sci. Pollut. Res. 28, 46781–46796. https://doi.org/10.1007/s11356-021-12665-8.

Rodríguez Gómez, M.J., Matías Prieto, J., Cruz Sobrado, V., Calvo Magro, P., 2021. Nutritional characterization of six quinoa (*Chenopodium quinoa* Willd) varieties cultivated in Southern Europe. J. Food Compos. Anal. 99, 103876. https://doi.org/10.1016/j.jfca.2021.103876.

Ruano, M.V., Ribes, J., Seco, A., Ferrer, J., 2012. An improved sampling strategy based on trajectory design for application of the Morris method to systems with many input factors. Environ. Model. Softw. 37, 103–109. https://doi.org/10.1016/j.envsoft.2012.03.008.

Ruiz, K.B., Biondi, S., Martínez, E.A., Orsini, F., Antognoni, F., Jacobsen, S.-E., 2016. Quinoa – a model crop for understanding salt-tolerance mechanisms in halophytes. Plant Biosyst. - Int. J. Deal. Asp. Plant Biol. 150, 357–371. https://doi.org/10.1080/11263504.2015.1027317.

SALib, 2024. Getting Started — SALib's documentation [WWW Document]. URL ⟨https://salib.readthedocs.io/en/latest/user_guide/getting-started.html⟩ (Accessed 1.20.25).

Shabala, S., Hariadi, Y., Jacobsen, S.-E., 2013. Genotypic difference in salinity tolerance in quinoa is determined by differential control of xylem Na+ loading and stomatal density. J. Plant Physiol. 170, 906–914. https://doi.org/10.1016/j.jplph.2013.01.014.

Sin, G., Gernaey, K., 2009. Improving the Morris method for sensitivity analysis by scaling the elementary effects: 19th European Symposium on Computer Aided Process Engineering – ESCAPE19. Computer-Aided Chemical Engineering Series. Comput. Aided Chem. Eng. 26, 925–930. https://doi.org/10.1016/S1570-7946(09)70154-3.

Van Genuchten, M., Hoffman, G., 1984. Analysis of crop salt tolerance data. Ecol. Stud. 51, 258–271.

Van Genuchten, M.Th, 1980. A closed-form equation for predicting the hydraulic conductivity of unsaturated soils. Soil Sci. Soc. Am. J. 44, 892–898. https://doi.org/10.2136/sssaj1980.03615995004400050002x.

Van Straten, G., De Vos, A.C., Rozema, J., Bruning, B., Van Bodegom, P.M., 2019. An improved methodology to evaluate crop salt tolerance from field trials. Agric. Water Manag. 213, 375–387. https://doi.org/10.1016/j.agwat.2018.09.008.

Van Straten, G., Bruning, B., De Vos, A.C., González, A.P., Rozema, J., Van Bodegom, P. M., 2021. Estimating cultivar-specific salt tolerance model parameters from multi-annual field tests for identification of salt tolerant potato cultivars. Agric. Water Manag. 252, 106902. https://doi.org/10.1016/j.agwat.2021.106902.

Vilcacundo, R., Hernández-Ledesma, B., 2017. Nutritional and biological value of quinoa (*Chenopodium quinoa* Willd.). Curr. Opin. Food Sci. 14, 1–6. https://doi.org/10.1016/j.cofs.2016.11.007.

Vrugt, J.A., 2016. Markov chain Monte Carlo simulation using the DREAM software package: theory, concepts, and MATLAB implementation. Environ. Model. Softw. 75, 273–316. https://doi.org/10.1016/j.envsoft.2015.08.013.

Vrugt, J.A., ter Braak, C.J.F., Diks, C.G.H., Robinson, B.A., Hyman, J.M., Higdon, D., 2009. Accelerating Markov Chain Monte Carlo simulation by differential evolution with self-adaptive randomized subspace sampling. Int. J. Nonlinear Sci. Numer. Simul. 10. https://doi.org/10.1515/ijnsns.2009.10.3.273.

Webber, H.A., Madramootoo, C.A., Bourgault, M., Horst, M.G., Stulina, G., Smith, D.L., 2010. Adapting the CROPGRO model for saline soils: the case for a common bean crop. Irrig. Sci. 28, 317–329. https://doi.org/10.1007/s00271-009-0189-5.
Werkgroep Waterwijzer Landbouw, 2018. Waterwijzer Landbouw: Instrumentarium voor kwantificeren van effecten van waterbeheer en klimaat op landbouwproductie.
Yazar, A., Incekaya, Ç., Sezen, S.M., Jacobsen, S.-E., 2015. Saline water irrigation of quinoa (Chenopodium quinoa) under Mediterranean conditions. Crop Pasture Sci. 66, 993. https://doi.org/10.1071/CP14243.